MOLECULAR AND CELLULAR BIOLOGY, Mar. 2011, p. 935–954 Vol. 31, No. 5
0270-7306/11/$12.00 doi:10.1128/MCB.00945-10

TIA1 Prevents Skipping of a Critical Exon Associated with Spinal Muscular Atrophy▽†

Natalia N. Singh,* Joonbae Seo, Eric W. Ottesen, Maria Shishimorova, Dhruva Bhattacharya, and Ravindra N. Singh*

Department of Biomedical Sciences, Iowa State University, Ames, Iowa 50011

Received 13 August 2010/Returned for modification 20 September 2010/Accepted 20 December 2010

Prevention of skipping of exon 7 during pre-mRNA splicing of *Survival Motor Neuron 2* (*SMN2*) holds the promise for cure of spinal muscular atrophy (SMA), a leading genetic cause of infant mortality. Here, we report T-cell-restricted intracellular antigen 1 (TIA1) and TIA1-related (TIAR) proteins as intron-associated positive regulators of *SMN2* exon 7 splicing. We show that TIA1/TIAR stimulate exon recognition in an entirely novel context in which intronic U-rich motifs are separated from the 5′ splice site by overlapping inhibitory elements. TIA1 and TIAR are modular proteins with three N-terminal RNA recognition motifs (RRMs) and a C-terminal glutamine-rich (Q-rich) domain. Our results reveal that any one RRM in combination with a Q domain is necessary and sufficient for TIA1-associated regulation of *SMN2* exon 7 splicing *in vivo*. We also show that increased expression of TIA1 counteracts the inhibitory effect of polypyrimidine tract binding protein, a ubiquitously expressed factor recently implicated in regulation of *SMN* exon 7 splicing. Our findings expand the scope of TIA1/TIAR in genome-wide regulation of alternative splicing under normal and pathological conditions.

Current estimates suggest that 95 to 100% of human genes with two or more exons are alternatively spliced, affecting all major aspects of cellular metabolism under normal and pathological conditions (12, 42). The mechanism of alternative splicing involves a complex combinatorial control in which exonic and intronic splicing enhancers (ESEs and ISEs, respectively), and silencers (ESSs and ISSs, respectively) play significant roles. In general, serine- and arginine-rich (SR) proteins promote exon inclusion through interactions with ESEs, whereas heteronuclear ribonucleoproteins (hnRNPs) promote exon exclusion through interactions with ESSs and ISSs (13, 34). Most of these proteins contain at least one RNA recognition motif (RRM) that is responsible for providing target specificity (11). Depending on the site of binding, SR proteins can also promote exon skipping, and hnRNPs can promote exon inclusion (17, 26). Alternative splicing is also regulated by several other factors not related to SR proteins and hnRNPs. In addition, RNA structures that directly or indirectly affect spliceosome assembly and catalytic core formation could modulate the outcome of splicing (42, 47).

The splicing reaction calls for the highest degree of precision since a shift in splicing position by 1 nucleotide could have devastating consequences (12). The biggest challenge in our understanding of alternative splicing emanates from our inability to fully comprehend the combinatorial control exerted by *cis* elements. Using functional or genomic approaches, a vast majority of studies have concentrated on deciphering the nature of *cis* elements located within exons (6, 27, 61, 63, 66). Very few studies have been dedicated to intronic *cis* elements, mostly focusing on the regions that flank exonic sequences (59, 65, 66, 69). Recent genome-wide analyses of intronic sequences revealed significant enrichment of U-rich motifs downstream of 5′ splice sites (3, 19). Furthermore, depletion of T-cell-restricted intracellular antigen 1 (TIA1) protein and TIA1-like 1 (TIAL1; also referred to as TIAR) protein has been found to promote exon skipping in genes containing U-rich stretches immediately downstream of the 5′ splice site (ss) particularly between +6 and +30 the intron positions (3). These findings are consistent with an earlier report in which TIA1 and TIAR showed preference for certain types of U-rich motifs *in vitro* (16). TIA1 is a modular protein which contains three RRMs at the N terminus and an auxiliary glutamine rich (Q-rich) domain at the C terminus (29, 57). Based on *in vitro* studies, it has been proposed that TIA1 recruits U1 snRNP through direct interactions with the U1 snRNP and U-rich intronic sequences adjacent to the 5′ ss (18). There is another study that suggested but did not conclusively prove that TIA1 may also be active from a greater distance from the 5′ ss (71). An earlier finding that *Saccharomyces cerevisiae* TIA1 homologue NAM8 is able to activate the 5′ ss from a longer distance may argue for a general role of TIA1 in splicing regulation in higher eukaryotes (67). Currently, it is not known if TIA1 could stimulate exon inclusion through binding to U-rich intronic sequences away from the 5′ ss in an altered context in which intronic sequences adjacent to the 5′ ss are known to be negative splicing regulators. In addition to the role of TIA1 in pre-mRNA splicing in the nucleus, another well-known TIA1 function pertains to stress granule formation and translation repression in the cytoplasm (1, 20). However, the mechanisms by which different

* Corresponding author. Mailing address: Department of Biomedical Sciences, College of Veterinary Medicine, 2034 Veterinary Medicine Bldg., Iowa State University, Ames, IA 50011. Phone for Ravindra N. Singh: (515) 294-8505. Fax: (515) 294-2315. E-mail: singhr@iastate.edu. Phone for Natalia N. Singh: (515) 294-2451. Fax: (515) 294-2315. E-mail: natalias@iastate.edu.

† Supplemental material for this article may be found at http://mcb.asm.org/.

▽ Published ahead of print on 28 December 2010.

TIA1 domains participate in critical *in vivo* events such as nucleo-cytoplasmic shuttling and protein-protein and protein-RNA interactions remain poorly understood.

Spinal muscular atrophy (SMA), the second most common autosomal recessive disorder, is caused by deletions or mutations of the *Survival Motor Neuron 1* (*SMN1*) gene (36). A nearly identical copy of the gene, *SMN2*, fails to compensate for the loss of *SMN1* because exon 7 is skipped, producing the truncated protein SMNΔ7, which is unstable (8, 31, 58). *SMN1* and *SMN2* differ by a critical C-to-T substitution at position 6 (C6U transition) of exon 7 in *SMN2*. C6U is sufficient to trigger exon 7 skipping due to a loss of an ESE associated with SF2/ASF and/or a gain of a silencer associated with hnRNP A1 (38, 44). Skipping of *SMN2* exon 7 is facilitated by a number of inhibitory elements clustered around the 5′ ss of exon 7. These include TSL2 (an inhibitory RNA structure sequestering the 5′ ss of exon 7), a 3′ cluster (an ESS), and intronic splicing silencer N1 (ISS-N1) that harbors two hnRNP A1 motifs (24, 48, 50, 51). ISS-N1 partially overlaps an 8-nucleotide-long GC-rich motif, which exerts its own inhibitory effect (52). Due to the direct significance for a major genetic disease, splicing of *SMN* exon 7 has become one of the most studied systems in humans. Consistently, several factors including Tra2-β1, SF2/ASF, hnRNP A1, hnRNP G, SRp30c, hnRNP Q1, and Sam68 have been shown to modulate *SMN* exon 7 splicing (7, 44, 56). Most of these factors interact directly or indirectly with sequences of exon 7. Recently, polypyrimidine tract binding protein (PTB) and far-upstream element (FUSE) binding protein have been shown to interact with element 1, a previously described inhibitory element within intron 6 of *SMN* (4). Two independent studies have resulted in the identification of ISEs within intron 7 (21, 41). However, factors interacting with these ISEs remain unknown. *SMN* exon 7 is flanked by an ~6-kb-long intron 6 and 444-base-long intron 7. Currently, there is no report of a splicing factor that promotes *SMN2* exon 7 inclusion by binding to an intronic sequence.

Here, we report TIA1 as a positive regulator of *SMN2* exon 7 splicing. It promotes exon 7 inclusion by binding to U-rich intronic motifs presented in a novel context where these motifs are separated from the 5′ ss by the strong inhibitory element ISS-N1. Our results expand the scope of splicing regulation by TIA1 and TIAR through a unique combinatorial control in which strict requirement of U-rich motifs adjacent to the 5′ ss is obviated. Using purified protein, we show that the affinity of two adjacent U-rich motifs within *SMN2* intron 7 is better than one of the best TIA1 binding sequences isolated by *in vitro* selection (16). We also demonstrate that the Q-rich domain in combination with any one of the three RRMs is necessary and sufficient for the stimulatory effect of TIA1 *in vivo*. Further, we show that the stimulatory effect of TIA1 offsets the inhibitory effect of PTB. This study constitutes the first report of *SMN* exon 7 splicing regulation by a Q-rich-domain-containing protein and brings a new perspective to splicing regulation of a critical housekeeping gene associated with a major genetic disease of children and infants.

MATERIALS AND METHODS

Plasmid constructs. Several of the minigene splicing cassettes and plasmids here have been described previously: pSMN1ΔI6 and pSMN2ΔI6 (49), SMN2ΔISS-N1, ISS-N1/M35, Casp3Avr and Casp3ISS-N1 (48), pTBEx12-50A (43), pTBApo-ISE3m (40), myc-PTB (62), SMN2I7Δ190–406, and Casp3SMN2 (53). In this study we refer to pSMN1ΔI6 and pSMN2ΔI6 as *SMN1* and *SMN2*. Generation of other clones has been described in the supplemental material. All primers were obtained from Integrated DNA Technologies (Coralville, IA). Deletions and site-specific mutations in the minigenes of interest were introduced by a strategy described earlier (48). A Casp3-exon7-ISS-N1 minigene was generated by replacing *Casp3* exon 6 with *SMN2* exon 7 and simultaneously inserting the ISS-N1 sequence 9 nucleotides downstream.

Human 3XFLAG-hTIA1 mammalian expression vector was generated as follows. Three copies of the FLAG tag (3XFLAG) sequence 5′-ATG GAC TAC AAA GAC CAT GAC GGT GAT TAT AAA GAT CAT GAC ATC GAC TAC AAA GAC GAC GAT GAC AAG *ACG CGT* TCT AGA-3′ (the downstream Mlu site is shown in italics and the XbaI site is underlined) were added (in frame) to the 5′ end of human TIA1 cDNA during a two-step PCR. PCR was performed using Phusion High-Fidelity DNA polymerase (New England BioLabs, Ipswich, MA) and human cDNA prepared from HeLa cells. The amplified sequence (3XFLAG tag followed by in-frame TIA1 cDNA sequence) was then cloned in the EcoRI-SalI restriction sites of a pCI-neo mammalian expression vector (Promega, Madison, WI). To distinguish between the full-length TIA1 and TIA1Δ5, *Escherichia coli* colonies were screened by PCR using *Taq* DNA polymerase (Invitrogen, Carlsbad, CA) and the primer pair 5′hTIA1 (5′-GCC CAA GAC TCT ATA CGT CGG TAA CC-3′) and 3′hTIA1 (5′-GGT GCA AAA GCA GCT TTT ATA TCT TC-3′). The 3XFLAG-hTIA1 plasmid digested with Mlu and SalI was subsequently used for cloning of different TIA1 domains as well as TIAR and TIARΔ3. Different domains of TIA1 were generated by PCR using 3XFLAG-hTIA1 as a template. The regions of the wild-type full-length TIA1 included in each 3XFLAG domain construct were the following: RRM1, amino acids (aa) 2 to 110; RRM2, aa 93 to 197; RRM3, aa 185 to 289 followed by 13 additional unrelated amino acids; Q, aa 260 to 386; RRM1+Q, aa 2 to 92 plus aa 273 to 386; RRM2+Q, aa 93 to 197 plus aa 272 to 386; RRM3+Q, aa 199 to 386; RRM1+2, aa 2 to 193 followed by 10 additional unrelated amino acids; RRM1+3, aa 2 to 92 plus aa 198 to 283; RRM2+3, aa 82 to 299; ΔRRM1, aa 82 to 386; ΔRRM2, aa 2 to 92 plus aa 198 to 386; ΔRRM3, aa 2 to 198 plus aa 278 to 386; RRM1+2+3, aa 2 to 299; TIA1ΔQ1, aa 2 to 367; TIA1ΔQ2, aa 2 to 349; TIA1ΔQ3, aa 2 to 329; TIA1ΔQ4, aa 2 to 309; TIA1ΔQ5b, aa 2 to 283; TIA1-3′Q, aa 2 to 293 plus 344 to 386; fusion 1a, aa 2 to 299 followed by 32 unrelated amino acids, and fusion 2b, aa 2 to 299 followed by a glutamine-rich segment of 33 unrelated amino acids. TIAR and TIARΔ3 sequences were amplified by reverse transcription-PCR (RT-PCR) using total RNA prepared from HeLa cells and the primer pair 5′MluhTIAR (5′-ACC AAG *ACG CGT* TCT AGA ATG GAA GAC GAC GGG CAG CCC CGG-3′) and 3′SalhTIAR (5′-CAT ATA TAT *GTC GAC* TCA CTG TGT TTG GTA ACT TGC CAT AC-3′) (Mlu and SalI sites are shown in italics). To distinguish between the full-length TIAR and TIARΔ3, *E. coli* colonies were screened using PCR with *Taq* DNA polymerase and the primer pair 5′hTIAR (5′-CAG AAG TCC TTA TAC TTC AGT TG-3′) and 3′hTIAR (5′-CTA ATG CAG CAG CTG CAT CTC TG-3′). All constructs were sequenced before their use. According to sequencing results, the generated 3XFLAG-hTIA1 construct has a silent mutation (GGC to GGT) at amino acid position 307.

Templates for T7 *in vitro* transcription were generated as follows. *SMN2* intron 7 sequences, wild type as well as those containing deletions/site-specific substitutions, were amplified from the corresponding *SMN2* minigenes using Phusion High-Fidelity DNA Polymerase and the following primer combinations: P167 (5′-GTA *TGG TAC C*TA ATA CGA CTC ACT ATA GGG TAA GTC TGC CAG CAT TAT GAA AG-3′) and P164 (5′-GCA T*AA GCT T*TT TAA ATG TTC AAA AAC ATT TG-3′) for wild type (WT), T7 with a deletion of residues 29 to 60 (T7Δ29-60), T7Δ25-34, T7Δ29-40, T7Δ37-48, T7Δ46-55, T7Δ50-60, T7Δ53-64, T7-URC2S3A (where URC2S3A is U-rich cluster 2 with substitutions for three U residues), T7-URC2S3B (where B indicates a substitution of three difference U residues in URC2), T7-URC2S6A, T7-URC2S4A, T7-URC1S2A, T7-URC1S4A, and T7-URC1S6A constructs; P167 and P165 (5′-GCA T*AA GCT T*TT TAA ACC ATA AAG TTT TAC AAA-3′) for the T7Δ56-82 construct; P167 and P166 (5′-GCA T*AA GCT T*TT TCA TTT GTT TTC CAC AAA CC-3′) for the T7Δ70-82 construct; and P167 and PΔ61-74 (5′-GCA T*AA GCT T*TT TAA ATG TTC TCC ACA AAC CA-3′) for T7Δ61-74 construct. In the above primers, T7 promoter sequence is underlined and KpnI/HindIII restriction sites are shown in italics. The generated PCR fragments were digested with KpnI and HindIII and cloned into the pUC19 vector. As a positive control in our filter binding assay, we used "sequence 1-1" reported to be a high-affinity TIA1 binder (16). The DNA template for RNA sequence 1-1 was generated by PCR using primers P187 (5′-GTA T*GG TAC C*TA ATA CGA CTC ACT ATA GGG TCT TTT TAA GTC GTA CCT AAT CC-3′) and P163 (5′-GCA T*AA GCT T*GG CCG TTC GAC GAG TAT ACA TCC

TAC-3′) and the oligonucleotide TEMP (5′-TTT AAG TCG TAC CTA ATC CTC GTC TCA GTG CCA TAG TGT AGG ATG TAT ACT CGT CGA AC-3′) as a template. In the above primers, T7 promoter sequence is underlined, and KpnI/HindIII sequences are shown in italics. A PCR fragment digested with KpnI and HindIII was cloned in the pUC19 vector. All plasmids were sequenced before their use.

Cell culture, siRNA, and ASOs. Unless otherwise stated, all tissue culture media and supplies were purchased from Invitrogen. HeLa cells were obtained from the American Type Culture Collection and were cultured in Dulbecco's modified Eagle's medium (DMEM) supplemented with 10% fetal bovine serum (FBS). Primary fibroblasts from an SMA type I patient (repository number GM03813) were obtained from Coriell Cell Repositories (Camden, NJ). These cells were grown in minimal essential medium (MEM) supplemented with 2 mM GlutaMAX-I and 10% FBS. Wild-type mouse embryonic fibroblasts (MEF) and TIA$^{-/-}$ cells were a kind gift from Paul Anderson (33). These cells were maintained in DMEM supplemented with 10% FBS. Small interfering RNAs ([siRNAs] custom or ON-TARGETplus SMARTpool) against the proteins of interest and antisense oligonucleotides (ASOs) used in this study were purchased from Dharmacon Inc. (Lafayette, CO). An ON-TARGETplus nontargeting pool was used as a negative siRNA control. A custom siRNA duplex targeting region from position 1022 to position 1044 was used to knock down TIAR. The ASOs incorporated 2′-*O*-methyl modification and phosphorothioate backbone as described earlier (48).

Cell transfections. Unless stated otherwise, cotransfections of cells with a protein expression vector, minigene of interest, and/or ASOs were performed using Fugene HD (Roche Applied Science, Indianapolis, IN) following the manufacturer's recommendations. Briefly, depending on the amount of HeLa cells needed for analysis, ~16 h before transfection they were plated in either a 24-well plate or 6-well plate at a density of 0.9×10^5 cells per well or 4.8×10^5 cells per well, respectively. The amounts of minigene DNA, protein expression vector, and ASO used are indicated in the figure legends. In each experiment the ratio between nucleic acids and Fugene HD was maintained at 1:3.5. Cells were collected 24 h after transfection. For total RNA preparation only, cells transfected in 24-well plates were washed with phosphate-buffered saline (PBS; Invitrogen) and lysed in Trizol reagent (Invitrogen) directly in each well. For simultaneous protein and RNA analysis, HeLa cells were transfected in six-well plates, washed with ice-cold PBS three times 24 h later, and collected by scraping. One-fourth of the cells were used for total RNA isolation, and the rest were used for making whole-cell extracts. If transfected cells were also needed for immunofluorescence (IF), we performed transfection of cells in 60-mm dishes (1.1×10^6 cells were plated per dish). At 6 to 8 h after transfection, cells were trypsinized, 1/12 of them were replated in 24-well plates containing glass coverslips to be used for IF, 1/4 were plated in six-well plates to be collected for total RNA preparation, and the rest of the cells were returned to 60-mm dishes to be collected for making whole-cell extracts as described above. For cytoplasmic and nuclear protein fractionation, HeLa cells were preplated in 100-mm dishes at a density of 3×10^6 cells per dish followed by transfection with 3XFLAG-hTIA1 plasmid ~16 h later. Cells were collected for fractionation and total RNA preparation 24 h after transfection. For RNA interference (RNAi), HeLa cells were transfected using Lipofectamine 2000 (Invitrogen). Here, the number of cells plated before transfection was increased to 5.5×10^5 cells per well of a six-well plate. Eight hours after transfection, cells in each well were trypsinized and divided among three wells for sample collection at 24 (total RNA), 48 (total RNA and protein), and 72 (total RNA) hours posttransfection. Transfection of MEF and TIA$^{-/-}$ cells with *SMN1*/*SMN2* minigenes was done using Lipofectamine 2000. These cells were plated at a density of 2.8×10^5 cells per well ~16 h prior to transfection. Lipofectamine 2000 was also used to transfect SMA patient fibroblasts GM03813 (plated at 1.5×10^5 cells per well) with ASOs.

RT-PCR analysis. Total RNA was isolated using Trizol reagent following the manufacturer's recommendations. To generate cDNA, reverse transcription was carried out using a SuperScript III reaction kit (Invitrogen). An oligo(dT) (Invitrogen) was used for pCI-based minigenes, while random hexamers (Invitrogen) were used for pTB vector-based minigenes. Generally, 0.8 to 3 μg of total RNA was used per 20 μl of RT reaction mixture. Minigene-specific spliced products were amplified using *Taq* DNA polymerase and the following primer combinations: P1 and P2 for *SMN* minigenes; alfa-23 and BRA2 for pTBXx9-V456F, pTBEx12-50A, and pTBApo-ISE3m minigenes; and P1 and P55 for *Casp3* minigenes (48). For PCR amplification of endogenous genes, we used the following pairs of primers: either N-24 and P2 (48) or P31 (5′-CAT GAG TGG CTA TCA TAC TG-3′) and P25 (5′-CTC GAA GCG GCC GCA GCT CAT AAA ATT ACC A-3′) for human *SMN* exon 7 and 5′Ex6-MoSmn (5′-CTG TCT GGA TGA CAC TGA TGC CC-3′) and 3′Ex8-MoSmn (5′-ACC CCA TCT CCT GAG ACA GAG C-3′) for mouse *Smn* exon 7. When cells were transfected with the *SMN2* minigene, PCR amplification of endogenous human *SMN* was performed using the primer combination N-23 (5′-CAC CGC CAC CAC CAC CCC ACT TA-3′) and P25 or N-24 and P26 (5′-GTA CAA TGA ACA GCC ATG TC −3′). PCRs were performed in the presence of a trace amount of [α-^{32}P]dATP (3,000 Ci/mmole; Perkin-Elmer Life Sciences, Oak Brook, IL). To distinguish spliced transcripts of *SMN2* from *SMN1*, the PCR products were subjected to digestion with DdeI (35). Analysis and quantifications of spliced products were performed using a FPL-5000 Image Reader and Multi Gauge software (Fuji Photo Film Inc., Valhalla, NY). Results were confirmed by at least three independent experiments.

Western blot analysis. Whole-cell extracts from HeLa cells were prepared using ice-cold radioimmunoprecipitation assay (RIPA) buffer (Boston BioProducts, Ashland, MA) supplemented with protease inhibitor cocktail (Roche Applied Science). Fractionations of cytoplasmic and nuclear proteins from HeLa cells and mouse embryonic fibroblasts were performed using an NE-PER Nuclear and Cytoplasmic Extraction kit (Pierce, Rockford, IL) following the manufacturer's instructions. The extraction reagents from the kit were supplemented with Halt protease inhibitor single-use cocktail (Thermo Scientific, Waltham, MA). Protein concentrations were determined using a bicinchoninic (BCA) protein assay kit (Thermo Scientific). Protein samples were resolved on an 11% SDS-polyacrylamide gel and transferred on polyvinylidene difluoride (Bio Trace PVDF) membrane (Pall Life Sciences, Ann Arbor, MI). The following primary and secondary antibodies were used: mouse monoclonal anti-FLAG M2 (Sigma-Aldrich, St. Louis, MO), mouse monoclonal anti-hnRNP Q (Sigma-Aldrich), mouse monoclonal anti-α-tubulin (Sigma-Aldrich), mouse monoclonal anti-β-actin (Sigma-Aldrich), rabbit polyclonal anti-Tra2 (Abcam Inc., Cambridge, MA), rabbit polyclonal to Myc tag (Abcam), rabbit polyclonal to histone H3 (Abcam), mouse monoclonal to glyceraldehyde-3-phosphate dehydrogenase (GAPDH; Abcam), mouse monoclonal to PTB1 (Abcam), mouse monoclonal to TATA binding protein (TBP; Abcam), goat polyclonal anti-TIA1 C-20 (Santa Cruz Biotechnology, Inc., Santa Cruz, CA), goat polyclonal anti-TIAR C-18 (Santa Cruz Biotechnology, Inc.), and horseradish peroxidase-conjugated secondary antibodies against mouse (Sigma-Aldrich), rabbit (Jackson ImmunoResearch, West Grove, PA), and goat (Santa Cruz Biotechnology, Inc.). In most cases, membranes were stripped (10 to 15 min at room temperature) using Restore Western Blot Stripping Buffer (Thermo Scientific) and reprobed. Immunoreactive proteins were visualized with SuperSignal West Dura Extended Duration Substrate (Pierce) or SuperSignal West Femto Maximum Sensitivity Substrate (Pierce). The membranes were scanned using a UVP BioSpectrum AC Imaging System (UVP, Upland, CA). Results were confirmed by at least three independent experiments.

***In vitro* binding assay.** Radiolabeled RNA probes used for the nitrocellulose filter binding assay were generated by *in vitro* transcription using HindIII-linearized plasmids and a MEGAshortscript T7 kit (Ambion) in the presence of [α-^{32}P]UTP (3,000 Ci/mmole; Perkin-Elmer Life Sciences). Sequence 1-1 was the same RNA as described by Dember et al. (16). Transcribed RNA probes were purified on a denaturing 6% polyacrylamide gel using the crush and soak method (48) and recovered by ethanol precipitation. Binding was performed similarly according to the method of Singh et al. (55). Briefly, a 100-μl reaction mixture in binding buffer (40 mM Tris-HCl, pH 7.5 containing 100 mM NaCl, 5 mM $MgCl_2$, 5 mM dithiothreitol [DTT], and 4% glycerol) containing 35 nM control RNA (either wild type or sequence 1-1), 70 nM mutant RNA, and 1 μM purified TIA1 was incubated for 20 min at room temperature. To capture protein-bound RNA, the reaction mixture was passed through a nitrocellulose membrane (Protran BA 85; Whatman Inc., Piscataway, NJ). The membrane was washed once with 800 μl of binding buffer followed by washing with high-salt buffer (binding buffer containing 450 mM NaCl). RNA bound to the membrane was eluted by phenol-chloroform extraction (150 μl of Tris-EDTA [TE] buffer plus 600 μl of phenol-chloroform), followed by ethanol precipitation in the presence of glycogen (Roche Applied Science), and analyzed on a denaturing 8% polyacrylamide gel, which was dried and quantified using a FPL-5000 Image Reader and Multi Gauge software (Fuji Photo Film Inc.). The binding affinity of a given mutant was compared with wild-type RNA using the following equation: [amount of bound^{RNA1}/(amount of bound^{RNA1} + amount of bound^{RNA2})]/[amount of input^{RNA1}/(amount of input^{RNA1} + amount of input^{RNA2})], where RNA1 is a mutant RNA and RNA2 is a control (wild type or sequence 1-1). The affinity of the mutant RNA compared to that of sequence 1-1 was corrected to the wild-type level using the following equation: affinity^{RNA1}/affinity^{WT}, where both affinities were determined by comparing binding reactions with sequence 1-1 as control.

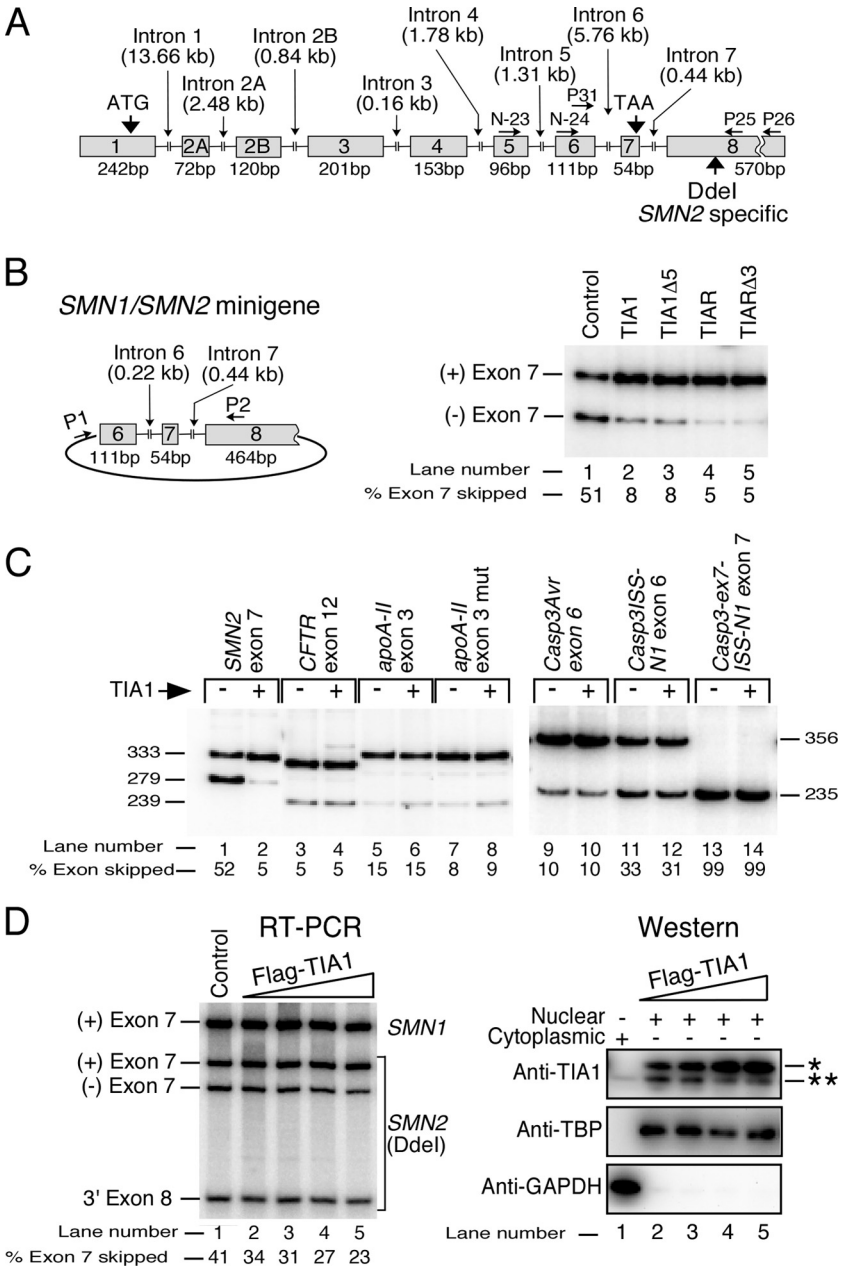

FIG. 1. Effect of TIA1 on *SMN* exon 7 splicing. (A) Schematic diagram of the *SMN* gene. Exons are shown as gray boxes and introns are shown as broken lines. Sizes of exons and introns are indicated. Locations of the start and stop codons as well as the *SMN2*-specific DdeI restriction site are indicated by bold vertical arrows. The annealing positions of primers used for amplifications of endogenous *SMN* transcripts are shown by horizontal arrows. (B) *In vivo* splicing pattern of the *SMN2* minigene in the presence of different nuclear proteins from the TIA1 family. A schematic diagram of the *SMN* minigenes is shown in the left panel. *SMN* exons are represented by gray boxes, and intervening introns are shown by broken lines. Sizes of exons and introns are indicated. Of note, intron 6 has been shortened to improve transfection efficiency (49). Annealing positions of primers for amplification of minigene-derived transcripts are shown. Results of *in vivo* splicing of the *SMN2* minigene are shown in the right panel. Data were generated employing HeLa cells grown in 24-well plates. Cells were cotransfected with 0.04 μg of *SMN2* and 0.46 μg of a 3XFLAG protein expression vector. Total RNA for the splicing assay was prepared from cells harvested 24 h posttransfection. Exon 7-included (+) and exon 7-skipped (−) spliced products are indicated. Results were analyzed as described previously (49). (C) *In vivo* splicing pattern of different minigenes in the presence of the overexpressed human full-length TIA1. HeLa cells plated in 24-well plates were cotransfected with 0.04 μg of a given minigene and 0.46 μg of either pCI-neo (empty vector) or 3XFLAG-hTIA1, and total RNA was prepared 24 h later. In every lane, upper and lower bands represent exon-included and exon-skipped products, respectively. In *CFTR*, *ApoA-II*, *Casp3Avr*, and *Casp3ISS-N1*, the major bands represent the exon-included products while in *Casp3-ex7-ISS-N1* the single band represents an exon-skipped product. Numbers on the left and right are sizes in base pairs. The percentage of exon skipping was calculated from the total value of exon-skipped and exon-included products. (D) Effect of TIA1 overexpression on endogenous *SMN* exon 7 splicing. HeLa cells plated in 100-mm dishes were transfected with increasing amounts of 3XFLAG-hTIA1 plasmid (2.0, 4.5, 9.0, and 18 μg). After 24 h cells were collected for total RNA preparation/protein fractionation. Splicing patterns of endogenous *SMN1* and *SMN2* are shown in the left panel. Spliced products were analyzed by RT-PCR using primers located in exon 6 (N-24 in panel A) and exon 8 (P25 in panel A). Following RT-PCR, DdeI digestion was performed to distinguish spliced

RESULTS

TIA1 restores *SMN2* exon 7 inclusion. As the first step toward evaluating the role of a Q-rich-domain-containing RNA binding protein on *SMN2* exon 7 splicing, we cotransfected HeLa cells with *SMN2* minigene and a mammalian expression vector harboring the complete coding sequence of human TIA1 or its near homologue TIAR. For the sake of clarity, diagrammatic representations of the *SMN* genes and minigenes have been given in Fig. 1A and B. Of note, exon 8 of *SMN2* contains a DdeI restriction site, which is absent in *SMN1*. Hence, RT-PCR followed by restriction digestion with DdeI distinguishes *SMN2* and *SMN1* transcripts (35) (Fig. 1D). Our initial screening was performed under nonlimiting concentrations of the expressed TIA1/TIAR by using a low minigene-to-expression vector ratio (Fig. 1B). Unless mentioned otherwise, all expressed proteins carried a 3XFLAG tag, and their expression levels were monitored by Western blotting employing antibodies against FLAG. Total RNA was prepared from cells harvested 24 h posttransfection, and the effect on *SMN2* exon 7 splicing was determined by RT-PCR. As shown in Fig. 1B, both TIA1 and TIAR were found to restore *SMN2* exon 7 inclusion. We next performed experiments with TIA1Δ5 and TIARΔ3, the predominant spliced variants of TIA1 and TIAR, respectively. These spliced variants are differentially regulated in different tissue types (28). Similar to their full-length counterparts, TIA1Δ5 and TIARΔ3 were able to effectively restore *SMN2* exon 7 inclusion (Fig. 1B). These results are consistent with the findings of our subsequent experiments in which much shorter variants of TIA1 were able to fully restore *SMN2* exon 7 inclusion (described below).

From here on we chose to focus on TIA1 and its potential role in the regulation of alternative splicing of *SMN2* exon 7. To confirm that the observed stimulatory effect of TIA1 is not due to a nonspecific response on general splicing, we examined *in vivo* splicing patterns of several additional minigenes in the presence of the overexpressed TIA1. Minigenes chosen for this experiment represented a variety of splicing cassettes that had full or partial exon inclusion or skipping properties. Our results revealed high target specificity in which TIA1 had no effect on splicing in any of the minigenes tested except *SMN2* (Fig. 1C). Noticeably, the overexpression of TIA1 produced no stimulatory effect on splicing of a hybrid minigene (Fig. 1C, *Casp3-exon7-ISS-N1*), in which *Casp3* exon 6 was exchanged with *SMN2* exon 7 and ISS-N1 was added 9 nucleotides downstream. These results indicate that TIA1-responsive motif(s) involved in stimulation of *SMN2* exon 7 inclusion is located outside this exon.

Next, we wished to test the effect of TIA1 on splicing of exon 7 of endogenous *SMN2*. For this, we transfected HeLa cells with increasing concentrations of the 3XFLAG-hTIA1 plasmid (Fig. 1D). Western blotting validated the expression of FLAG-tagged protein in the nuclear extract (Fig. 1D). Of note, expressed 3XFLAG-hTIA1 was distinguishable from endogenous TIA1 due to a difference in size. Endogenous *SMN2* transcripts were amplified by RT-PCR employing a unique primer combination followed by DdeI digestion. Even with the 2-fold increase in expression of 3XFLAG-hTIA1 over endogenous TIA1, a decrease in *SMN2* exon 7 skipping was noticed (Fig. 1D). With approximately a 10-fold increase in 3XFLAG-hTIA1 expression, more than a 30% decrease in *SMN2* exon 7 skipping was recorded.

Increased *SMN* exon 7 skipping in TIA1 knockout cells. To further validate the role of TIA1 on *SMN* exon 7 splicing, we took advantage of an embryonic fibroblast cell line derived from TIA1 knockout mice (TIA1$^{-/-}$) (33). Nuclear extract from TIA1$^{-/-}$ cells confirmed complete depletion of TIA1 and slightly elevated levels of TIAR (Fig. 2A). Amplification of endogenous mouse *Smn* transcripts did not show exon 7 skipping in either cell line (Fig. 2B). When wild-type and TIA1$^{-/-}$ cells were transfected with the *SMN1* or *SMN2* minigene, we observed a >10% increase in *SMN1* and *SMN2* exon 7 skipping in TIA1$^{-/-}$ cells (Fig. 2C). Given the multitude of stimulatory splicing factors responsible for *SMN* exon 7 inclusion, a reproducible decrease of >10% in exon 7 inclusion in TIA1$^{-/-}$ cells is significant. This finding supports the idea that TIA1 is involved in regulation of exon 7 splicing, and the loss of this protein cannot be fully compensated by other splicing factors with redundant functions. The interesting observation that depletion of TIA1 was found to have no adverse effect on splicing of *Smn* exon 7 suggests that a TIA1-responsive motif involved in promotion of *SMN* exon 7 inclusion might be specific to humans. There are substantial differences between human and mouse introns that flank exon 7 (Fig. 2D). For instance, mouse intron 6 is about half the size of human intron 6, whereas mouse intron 7 is more than three times larger than human intron 7. Further, we have recently shown that a C residue at the 10th intronic position (^{10}C) of *SMN* intron 7 forms a long-distance negative interaction with the downstream intronic sequences. The ^{10}C-mediated long-distance interaction is very specific to position as well as residue and appears to be absent in the mouse (53). There are additional differences between human and mouse sequences immediately downstream of the 5′ ss of exon 7 (Fig. 2E). The significance of some of these sequences including ISS-N1 and overlapping GC-rich sequence has been described earlier (48, 52). In particular, human-specific ISS-N1 and GC-rich motifs weaken the 5′ ss of *SMN* exon 7 (48, 52).

Depletion of TIA1 promotes *SMN2* exon 7 skipping. To assess the impact of reduced levels of TIA1 on *SMN2* exon 7 splicing, we used an RNA interference-based approach. Here, HeLa cells were cotransfected with siRNAs of interest and the *SMN2* minigene. Samples were collected at 24 h, 48 h, and 72 h

products from *SMN2* (35). *SMN1* and *SMN2* spliced products with exon 7 included or skipped are indicated. The percentage of *SMN2* exon 7 skipping was calculated from the total value of *SMN2* exon-skipped and exon-included products. Control refers to untransfected cells. The results of Western blotting are shown in the right panel. Nuclear and cytoplasmic fractions are marked. A total of 15 μg of protein was used for nuclear and cytoplasmic samples. Primary antibodies used for probing are indicated on the left. Bands corresponding to FLAG-tagged (*) and endogenous (**) TIA1 are marked on the right. TATA binding protein (TBP) served as a nuclear marker, whereas GAPDH served as a cytoplasmic marker. Cytoplasmic fraction from untransfected cells was used as a negative and positive control for nuclear and cytoplasmic markers, respectively.

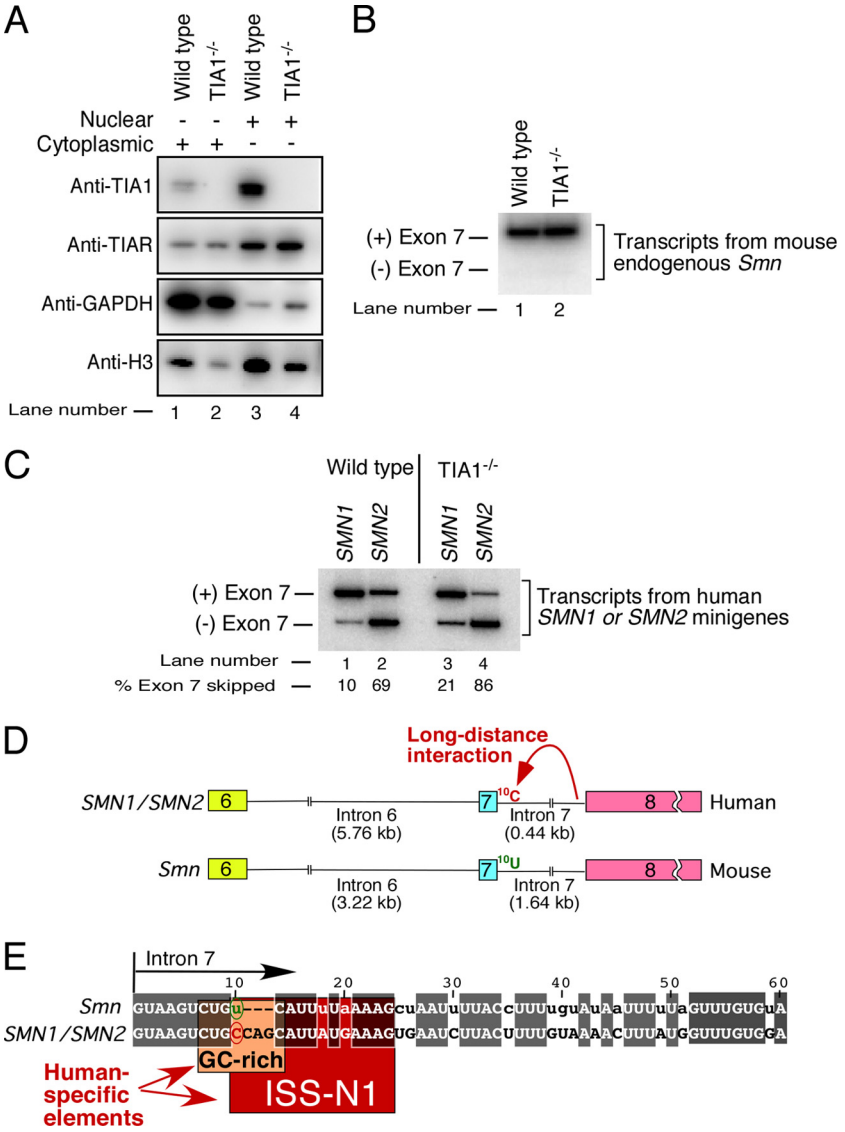

FIG. 2. Effect of TIA1 knockout on splicing of *SMN* exon 7. (A) Western blot showing levels of TIA1 and its homolog TIAR in wild-type and in TIA1$^{-/-}$ knockout mouse embryonic fibroblasts. Cellular proteins were fractionated, and 15 μg of protein of the nuclear/cytoplasmic fractions was used for SDS-PAGE. Primary antibodies used for probing are indicated on the left. GAPDH and histone 3 (H3) were used as markers for cytoplasmic and nuclear fractions, respectively. (B) Splicing pattern of mouse endogenous *Smn* exon 7 in TIA1$^{-/-}$ knockout mouse embryonic fibroblasts. Total RNA was prepared from wild-type or TIA1$^{-/-}$ knockout mouse embryonic fibroblasts, DNase treated and used for RT-PCR. One microgram of total RNA was used per 20 μl of reverse transcriptase reaction mixture. For the PCR step, mouse-specific primers annealing to exons 6 and 8 were employed. PCR amplification was done for 22 cycles; PCR products were ethanol precipitated and resolved on a native 5% PAGE gel. (C) *In vivo* splicing patterns of *SMN1* and *SMN2* minigenes in mouse embryonic fibroblasts. Mouse embryonic fibroblasts (wild type or TIA1 knockout) were transfected with 1 μg of *SMN1* or *SMN2* minigene and collected for total RNA preparation 24 h later. Spliced products were analyzed by RT-PCR as described in the legend of Fig. 1B. (D) Comparison of introns 6 and 7 of human (*SMN*) and mouse (*Smn*) genes. Exons are shown as colored boxes, and introns are shown as broken lines. Sizes of introns are given. ^{10}C, a human intronic nucleotide involved in long-distance interactions, is shown (53). (E) Alignment of the 5′ end of human and mouse intron 7. Numbering starts from the beginning of the intron. Nucleotides identical between human and mouse are highlighted in gray. Nonconserved mouse residues are shown in lowercase letters. The 10th intronic position is circled. ISS-N1, GC-rich sequence, and ^{10}C are specific to humans (48, 52, 53).

posttransfection, and the splicing patterns of both endogenous and minigene-derived *SMN2* pre-mRNAs were tested. The level of TIA1 protein was examined by Western blotting 48 h posttransfection. Considering that TIA1 displays functional redundancy with TIAR, including the ability to promote *SMN2* exon 7 inclusion (Fig. 1B), we also sought to test splicing of *SMN2* exon 7 when TIAR was knocked down. As a positive control, we used siRNAs against hnRNP Q1 and Tra-2β that have been previously shown to promote *SMN2* exon 7 inclusion (7, 23). In addition, siRNAs against all four proteins (TIA1, TIAR, hnRNP Q1, and Tra-2β) were simultaneously used for transfection. A nonfunctional siRNA pool served as a negative control. All siRNA experiments were successful in depleting their respective proteins, as indicated by the results of Western

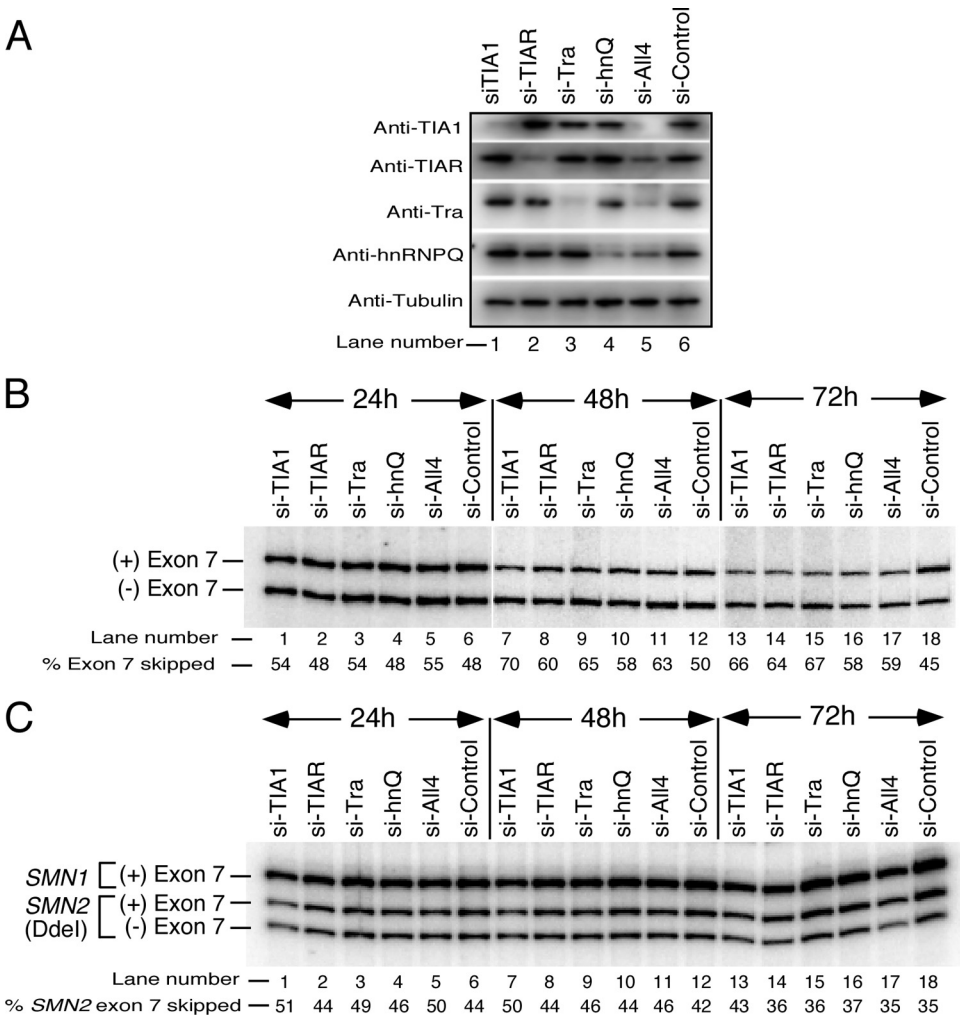

FIG. 3. Effect of depletion of TIA1 and other stimulatory proteins on *SMN* exon 7 splicing. (A) Western blot showing the effect of the indicated siRNAs on the level of corresponding proteins. HeLa cells were cotransfected with 1 μg of the *SMN2* minigene, and either 100 nM individual siRNA or all siRNAs simultaneously (25 nM each); whole-cell lysates were prepared 48 h after transfection. Primary antibodies used for probing are indicated on the left. (B) Time course of siRNA effect on splicing of *SMN2* minigene-derived exon 7. Cotransfections were done as described in panel A. Spliced products were analyzed by RT-PCR using minigene-specific primers, and total RNA was isolated from cells collected 24, 48, and 72 h after transfection. (C) Time course of siRNA effect on splicing of endogenous *SMN* exon 7. Cotransfections were done as described in panel A. Spliced products were analyzed by RT-PCR as described in panel B except that different primers, one located in exon 5 (N-23) and the other in exon 8 (P25), were used. Following RT-PCR, DdeI digestion was performed to distinguish spliced products from *SMN2* (35). The percentage of *SMN2* exon 7 skipping was calculated as in Fig. 1D.

blotting (Fig. 3A). Depletion of TIA1 resulted in a noticeable increase in *SMN2* exon 7 skipping from transcripts derived from the minigene (Fig. 3B). The effect was more pronounced at 48 h posttransfection since we observed more than a 40% increase in *SMN2* exon 7 skipping (calculated from a base value of the si-control sample). As expected, depletion of Tra2-β, TIAR, and hnRNP Q also promoted exon 7 skipping from *SMN2* minigene-derived transcripts. However, depletion of TIA1 had the greatest negative impact on *SMN2* exon 7 splicing. Interestingly, the simultaneous depletion of all four splicing proteins (TIA1, TIAR, hnRNP Q, and Tra2-β) did not produce a synergistic negative effect, suggesting that the above factors do not interact among each other to induce *SMN2* exon 7 inclusion (Fig. 3B). It is possible that simultaneous depletion of these factors may have upregulated other proteins with redundant splicing functions. It is also probable that reduced levels of one or more factors may have downregulated negative splicing factors.

As for the transcripts derived from endogenous *SMN2*, depletion of TIA1 resulted in ~20% increase in skipping of exon 7 (Fig. 3C, DdeI-digested bands). These results are consistent with the results of increased skipping of *SMN2* exon 7 in the TIA1$^{-/-}$ cells (Fig. 2C). We found that the effect of TIA1 depletion on endogenous *SMN2* exon 7 splicing was weaker than the effect on splicing of minigene-derived transcript. The differential response between the *SMN2* minigene and endogenous *SMN2* could be in part due to differences in the upstream context including a large promoter sequence through which additional factors may be recruited to the endogenous pre-mRNA. Indeed, a recent report suggested that the pro-

moter region has a role in regulation of *SMN* exon 7 splicing (39). Overall, the results of TIA1 depletion support a stimulatory role of this protein in *SMN2* exon 7 splicing.

TIA1 binding site is located downstream of ISS-N1. Published reports suggest that TIA1 exerts its function in splicing by directly interacting with a U-rich sequence immediately downstream of the 5′ ss of the affected exon. However, there are no U-rich motifs immediately downstream of the 5′ ss of *SMN* exon 7. Furthermore, our earlier finding that sequestration of either the GC-rich motif or ISS-N1 fully restores *SMN2* exon 7 inclusion ruled out the possibility that there is a stimulatory motif within the first 24 residues of intron 7 (48, 52). Therefore, we focused on intronic sequences downstream of ISS-N1. We started by generating *SMN2* mutant minigenes with large intron 7 deletions and testing their *in vivo* splicing patterns in the presence of overexpressed TIA1. Unless mentioned otherwise, these experiments were performed at an optimized 1:3 ratio of minigene to 3XFLAG-tagged hTIA1 vector. As shown in Fig. 4A, the *SMN2* mutant with a deletion of residues 190 to 406 in intron 7 (I7Δ190–406) that eliminated most of the 3′ half of intron 7 caused an improvement in exon 7 inclusion compared to that of the wild-type *SMN2*. This mutant responded positively to the overexpression of TIA1, suggesting that the binding site of TIA1 is not present in the deleted region. In contrast, *SMN2* mutant I7Δ30–100 almost entirely lost the ability to include exon 7 with or without overexpressed TIA1, suggesting that this region encompasses one or more positive regulators (Fig. 4A). To clarify that the TIA1 binding site is distinct from the previously described element 2 located in this region (41), we created *SMN2* constructs in which either element 2 or an area upstream was deleted (Fig. 4A, mutants I7Δ56–82 and I7Δ29–60). While I7Δ56–82 retained the ability to respond to TIA1, albeit with less efficiency, I7Δ29–60 became completely refractory to the overexpression of the protein (Fig. 4A). Thus, the region between ISS-N1 and element 2 emerged as the binding site for TIA1. Of note, more than 50% of the nucleotides in this region are U residues (Fig. 4B).

When site-specific mutations (deletions or substitutions) are used as an approach to find a potential binding site for a splicing factor, there is a possibility that deletion or substitution within the wild-type sequence may abrogate a sequence/structure motif or/and create a new motif. To confirm that I7Δ29–60 indeed disrupted TIA1 binding, we performed an antisense oligonucleotide (ASO) microwalk in which ASOs blocking overlapping targets downstream of ISS-N1 were used. Here, the *SMN2* minigene was cotransfected with an ASO of interest in the presence or absence of a TIA1 expression vector. A nonspecific ASO was used as a negative control. Confirming the stimulatory nature of the region, three out of four ASOs increased *SMN2* exon 7 skipping (Fig. 4B). A fourth ASO (24Dn16) that blocked the longest non-U-rich tract did not have any appreciable consequence on exon 7 splicing (Fig. 4B, lane 5). As shown in Fig. 4B, the overexpression of TIA1 promoted a dramatic increase in exon 7 inclusion only in the presence of the control ASO, while in the presence of 14Dn16, 29Dn16, and 35Dn15 most of exon 7 skipping was retained. Even the "ineffective" 24Dn16 noticeably decreased the positive effect of TIA1 (Fig. 4B). These results provided strong corroborative evidence in support of the location of TIA1 biding site between ISS-N1 and element 2.

Using an ASO-based approach we next tested whether a TIA1-associated intronic *cis* element was still required in the absence of ISS-N1, a major inhibitory element responsible for *SMN2* exon 7 skipping. Here, we transfected an ASO of interest with *SMN2* mutant minigenes in which ISS-N1 was either deleted or moved away from the 5′ ss (48) (see Fig. S1 in the supplemental material). Despite the loss of ISS-N1, the region between ISS-N1 and element 2 retained its stimulatory effect. This was most obvious in case of 29Dn16 that caused predominant skipping of *SMN2* exon 7 with or without overexpression of TIA1 (see Fig. S1B). These results revealed that TIA1 is an essential splicing factor for full restoration of *SMN2* exon 7 inclusion. Consistently, 29Dn16 led to a significant increase in exon 7 skipping from endogenous *SMN2* in several cell lines tested (see Fig. S1C and D).

URC1 and URC2 collaborate to promote TIA1-associated inclusion of *SMN2* exon 7 splicing. The sequence specificity of RRM-containing proteins generally comes from direct interactions of RRMs with a small stretch of nucleotides (11). Based on our results (Fig. 4), U-rich sequences downstream of ISS-N1 emerged as the likely sites for direct interactions with TIA1. As shown in Fig. 5A, the region starting immediately downstream of ISS-N1 and ending with element 2 contains three of what we called U-rich clusters or URCs (delineated based on the occurrence of U runs). To narrow down the potential binding site of TIA1, we generated a series of *SMN2* mutant minigenes with shorter (10 to 14 nucleotides) overlapping deletions that covered the above-mentioned region (Fig. 5A) and tested their *in vivo* splicing patterns in the presence or absence of overexpressed TIA1. URC1 contains UCUU, UU NCUUU, and CUUUU motifs. Interestingly, the last two have been shown to be significantly enriched downstream of the 5′ ss of constitutive and alternative exons (3). URC2 contains two UUU motifs separated by an AUGG stretch. As shown in Fig. 5, major deletions within URC1 or URC2 substantially reduced the ability of TIA1 to restore *SMN2* exon 7 inclusion, suggesting the additive effect of these motifs. In contrast, deletions between URC1 and URC2 did not affect the ability of TIA1 to restore *SMN2* exon 7 inclusion. These findings are consistent with the results of the antisense microwalk (Fig. 4B) and suggest that URC1 and URC2 are the sites of direct interaction with TIA1. One of our deletion mutations that created a longer URC by bringing URC1 closer to URC2 fully retained the stimulatory effect of TIA1 (Fig. 5, mutant I7Δ37-48). On the other hand, deletion of 10 nucleotides (UUUAU GGUUU) that eliminated both UUU motifs within URC2 substantially reduced the stimulatory effect of TIA1 (Fig. 5, mutant I7Δ46-55). Consistently, replacement of two UUU motifs within URC2 with nonuridine nucleotides almost completely eliminated TIA1-associated stimulatory response (Fig. 5, mutant URC2S6A).

To corroborate the results of deletion mutations, we then tested a large number of substitutions introduced in URC1/URC2 using an unbiased approach of sequence randomization at selected positions. Most of the substitutions reduced the stimulatory effect of overexpressed TIA1 on *SMN2* exon 7 splicing (Fig. 5; see also Fig. S2 and S3 in the supplemental material). Interestingly, a 3-nucleotide substitution that re-

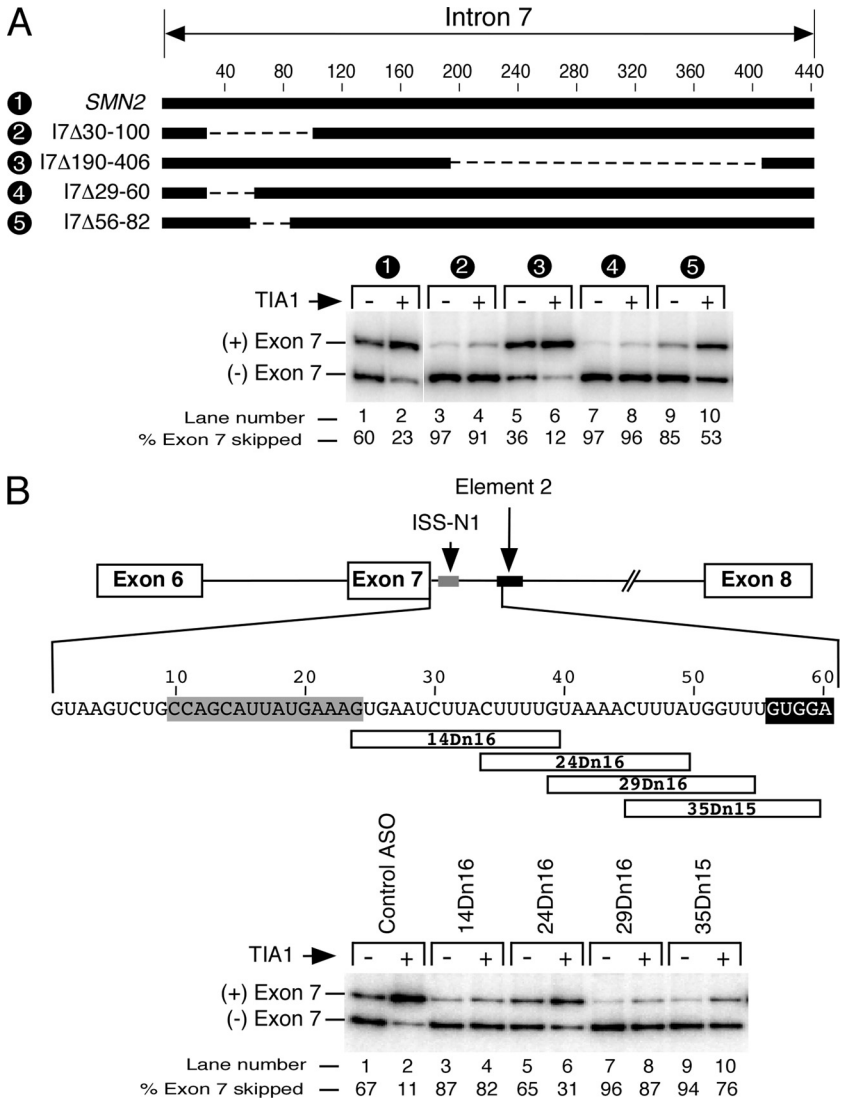

FIG. 4. Identification of intronic sequences responsible for TIA1-associated stimulatory effect on *SMN2* exon 7 splicing. (A) Effect of deletions in intron 7 on the ability of TIA1 to promote inclusion of *SMN2* exon 7. Diagrammatic representation of deletions within intron 7 of the *SMN2* minigene is given. Numbering of nucleotides starts from the first position of intron 7. Deletions are represented by dotted lines. Names of mutants are given on the left. Numbers in the names represent positions of the first and the last deleted nucleotides. *In vivo* splicing patterns of the wild-type *SMN2* minigene and intron 7 deletion mutants in the absence and presence of overexpressed TIA1 are shown in the lower panel. HeLa cells grown in 24-well plates were cotransfected with 0.04 μg of a given minigene and 0.118 μg of either empty vector or 3XFLAG-hTIA1. This amount of 3XFLAG-hTIA1 plasmid is similar to the lowest concentration used in the experiment shown in Fig. 1D downscaled to a 24-well plate. Results were analyzed as described in the legend of Fig. 1B. (B) Splicing pattern of the *SMN2* minigene cotransfected with different ASOs targeting sequences between ISS-N1 and element 2. Diagrammatic representation of ASOs and their annealing positions are given. Numbering of nucleotides starts from the first position of intron 7. ISS-N1 (gray) and element 2 (black) sequences are demarcated. ASOs are shown as horizontal bars. The lower panel shows the *in vivo* splicing pattern of the *SMN2* minigene in the presence of different ASOs with (+) or without (−) overexpressed TIA1. Experiments were performed with HeLa cells cotransfected with 0.04 μg of minigene, a 100 nM concentration of a given ASO, and 0.2 μg of either an empty vector or 3XFLAG-hTIA1. Results were analyzed as described in the legend of Fig. 1B.

placed UUU residues with CAC residues between the 53rd and 55th position of intron 7 had a substantial negative effect on *SMN2* exon 7 splicing (Fig. 5B, lane 25). Also, this mutant responded poorly to the overexpression of TIA1 (Fig. 5B, lanes 25 and 26). Our results once again confirmed that URC1 and URC2 are responsible for the TIA1-mediated increase in *SMN2* exon 7 inclusion. These results also underscored the significant finding that the TIA1-associated stimulatory function of U-rich motifs is exerted from beyond the 50th position of an intron.

URC1/URC2-linked stimulatory effect of TIA1 is portable. To validate that the stimulatory effect of TIA1 on *SMN2* exon 7 splicing *in vivo* is independent of sequences downstream of URC2, we used a hybrid minigene *Casp3SMN2* (53). In this minigene, the alternatively spliced *Casp3* exon 6 and its flanking intronic sequences were replaced with *SMN2* exon 7 and its

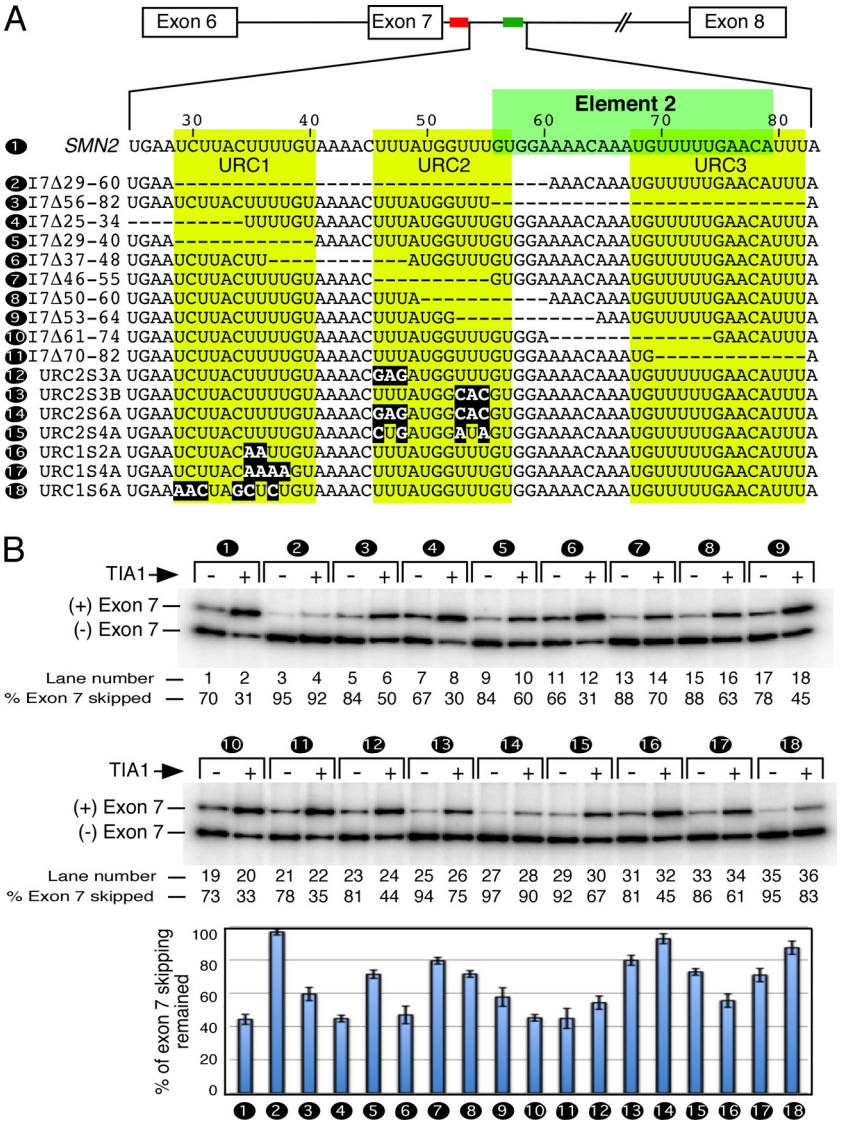

FIG. 5. Role of URC1 and URC2 on the TIA1-associated stimulatory effect on *SMN2* exon 7 splicing. (A) Diagrammatic representation of mutations within intron 7 of the *SMN2* minigene. Numbering of nucleotides starts from the first position of intron 7. Deletions are represented by dotted lines. Site-specific mutations are highlighted in black. Names of mutants are given on the left. Numbers in the names of deletion mutants represent positions of the first and the last deleted nucleotides. ISS-N1, element 2, and URCs are highlighted in red, green, and chartreuse yellow, respectively. (B) *In vivo* splicing pattern of the *SMN2* mutants shown in panel A. Cotransfection and splicing analysis were done similar to the method described in the legend of Fig. 4A. The bar diagram shown in the bottom panel represents residual exon 7 skipping for different mutants in the presence of 3XFLAG-hTIA1. Results in the bar diagram are expressed as per the following equation: 100 × [(exon 7 skipped in the presence of TIA1)/(exon 7 skipped in the absence of TIA1)]. Error bars based on standard deviation have been indicated. Standard deviation was determined based on three independent experiments performed in duplicates.

flanking intronic sequences, including 116 nucleotides of upstream intron 6 and 99 nucleotides of the downstream intron 7 (Fig. 6A). This exchange created a context in which splice sites of exons upstream and downstream of *SMN2* exon 7 substantially differed from the wild-type *SMN2*. As shown in Fig. 6B, splicing of *Casp3SMN2* produced predominant skipping of *SMN2* exon 7, but the overexpression of TIA1 was accompanied by an increase in inclusion of this exon. Gradual deletion of element 2 had no apparent effect on the ability of TIA1 to promote exon 7 inclusion (Fig. 6B, minigenes *Casp3*HYBΔ83–99, *Casp3*HYBΔ65–99, and *Casp3*HYBΔ56–99). However, deletion of sequences that included URC1 and URC2 in the absence or presence of element 2 led to a drastic decrease in the stimulatory response of overexpressed TIA1 (Fig. 6B, *Casp3*HYBΔ40–99, *Casp3*HYBΔ25–99 and *Casp3*HYBΔ29–60). These results are in full agreement with the results in the wild-type context in which deletion of sequences between ISS-N1 and element 2 led to a nearly total loss of *SMN2* exon 7 inclusion that could not be rescued by overexpression of TIA1 (Fig. 5). Deletion of URC1 alone (*Casp3*HYBΔ29–41, the hybrid *Casp3* minigene with deletion of residues 29 to 41) in the heterologous context reduced the ability of TIA1 to promote *SMN2* exon 7 inclusion compared to the wild-type context (Fig. 6C). Interestingly, ASO-medi-

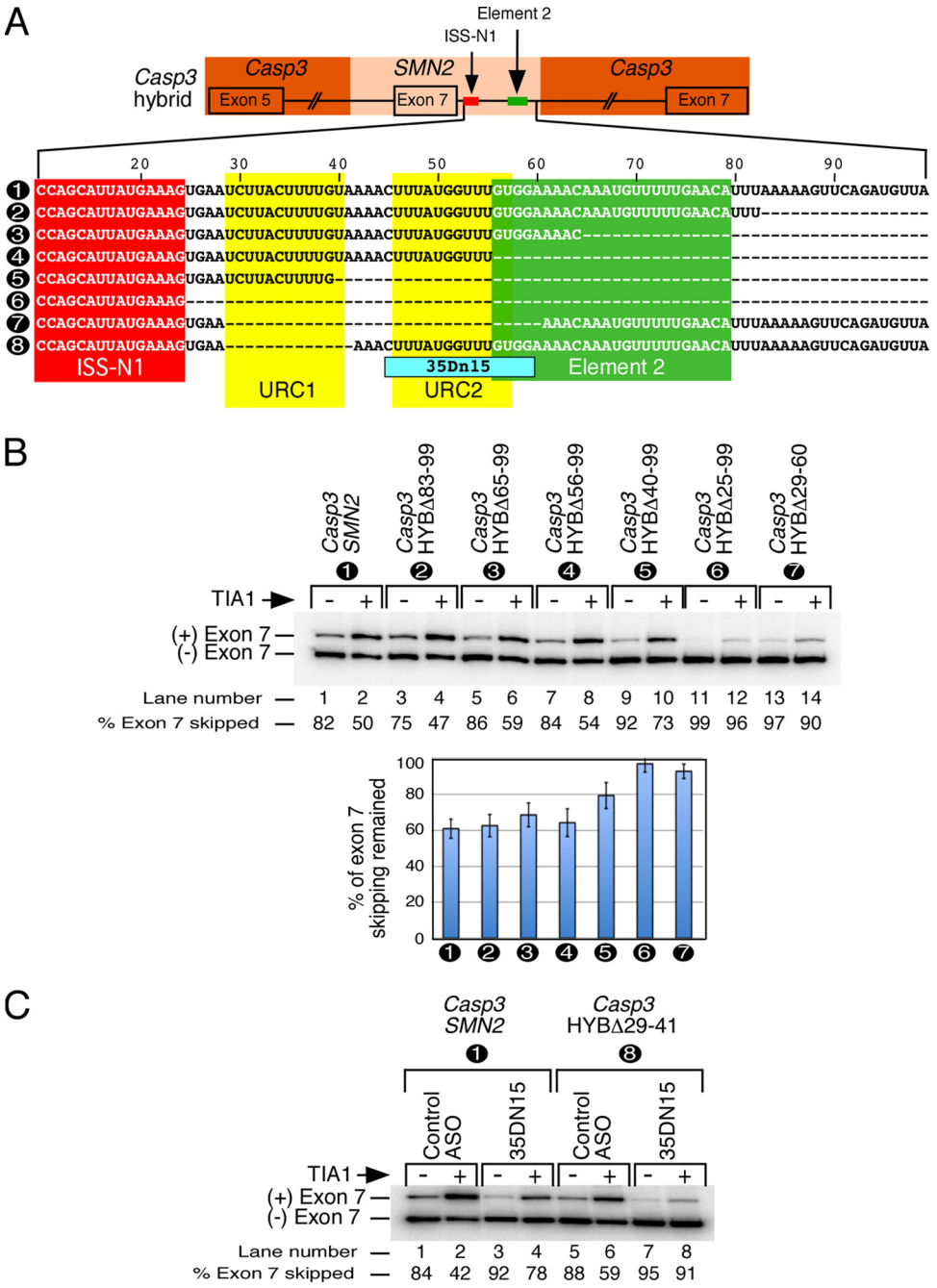

FIG. 6. Portability of TIA1-associated stimulatory response of URC1/URC2 in a heterologous context. (A) Diagrammatic representation of the *Casp3SMN2* hybrid minigene and its mutants. *Casp3* and *SMN2* sequences in the minigene are highlighted in dark and light red, respectively. Numbering of nucleotides starts from the first position of *SMN2* intron 7. ISS-N1, element 2, and URCs are highlighted in red, green, and yellow, respectively. Deletions are represented by dotted lines. Numbers in the names of the hybrid minigenes represent positions of the first and the last deleted nucleotides. ASO 35Dn15 is indicated by a blue horizontal bar, and its annealing position is shown. (B) *In vivo* splicing pattern of hybrid minigenes shown in panel A in the presence of overexpressed TIA1. HeLa cells grown in 24-well plates were cotransfected with 0.04 μg of a given hybrid minigene and 0.36 μg of either an empty vector or 3XFLAG-hTIA1. Splicing analysis was done similarly as described in the legend of Fig. 4A. The bar diagram shown in the bottom panel represents residual exon 7 skipping for different mutants in the presence of 3XFLAG-hTIA1. Results in the bar diagram were expressed as described in the legend of Fig. 5B. Error bars based on standard deviation have been indicated. (C) *In vivo* splicing patterns of *Casp3SMN2* and *Casp3*HYBΔ29–41 in the presence of TIA1 and a URC2-targeting ASO. HeLa cells grown in 24-well plates were cotransfected with 0.04 μg of minigene, a 100 nM concentration of a given ASO, and 0.36 μg of either an empty vector or 3XFLAG-hTIA1. Results were analyzed as described in the legend of Fig. 1B. Error bars were generated from standard deviations similar to the method described in the legend of Fig. 5B.

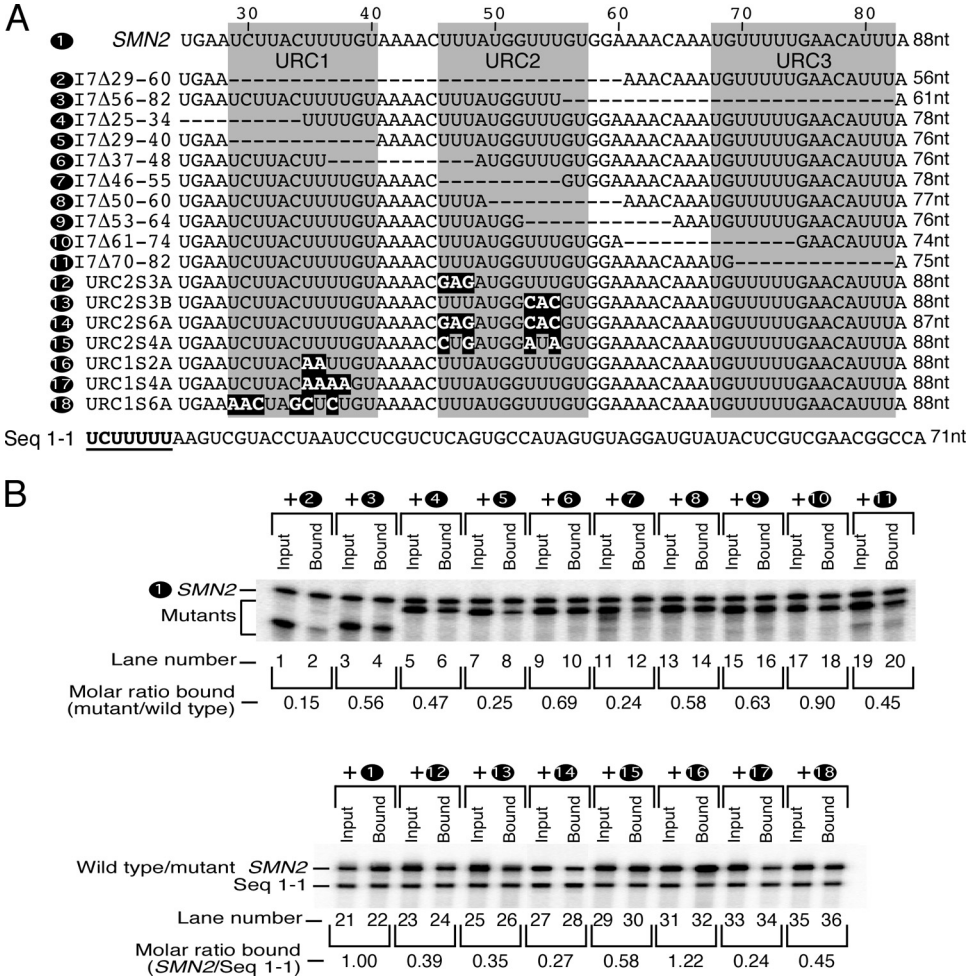

FIG. 7. *In vitro* binding of purified TIA1 with RNA substrates harboring URC1 and/or URC2. (A) Diagrammatic representation of RNA transcripts used for *in vitro* binding. Deletions in transcripts are represented by dotted lines. Site-specific mutations are highlighted in black. Names of transcripts are given on the left, and their lengths are shown on the right. URC1, URC2, and URC3 are highlighted in gray. Sequence 1-1 (seq 1-1) is a high-affinity ligand reported earlier (16). (B) Relative affinity of TIA1 for different RNA substrates described in panel A. Employing a nitrocellulose filter assay, binding strengths of different RNA substrates were compared with either wild-type sequence (upper panel) or sequence 1-1 (lower panel). Results were expressed by computing the fraction of input RNA substrate bound to the membrane against a common competing RNA (55). The bound molar ratio of each mutant was compared with the wild-type construct, the value for which was assigned as 1.

ated blocking of URC2 in the context of deleted URC1 led to a nearly complete loss of *SMN2* exon 7 inclusion even in the presence of overexpressed TIA1 (Fig. 6C, lanes 7 and 8). With selective blocking of URC2 only some of the stimulatory effect of TIA1 was retained (Fig. 6C, lanes 3 and 4). These results once again confirmed the additive effect of URC1 and URC2 on the TIA1-associated stimulatory response on *SMN2* exon 7 inclusion. Of note, to observe the stimulatory effect of TIA1 in a heterologous context comparable to the one produced in wild-type (*SMN2* minigene) context, we used three times as much of the TIA1 expression vector. While our results confirmed the portability of the TIA1-associated stimulatory effect of intronic U-rich sequences away from the 5′ ss, they also indicated the complexity of the exon definition process in which context-specific determinants including sequences downstream of URC2 would have influenced the degree of the stimulatory effect of TIA1.

***In vitro* binding supports affinity of TIA1 to URC1 and URC2.** To appreciate the specificity of the direct interaction between TIA1 and sequences downstream of ISS-N1, we performed *in vitro* binding employing purified TIA1 and RNA substrates with URC1 and URC2 motifs. The recombinant TIA1 was purified using the Impact system, which allows production of tag-free proteins in a single chromatographic step (10) (see Fig. S4 in the supplemental material). The wild-type *SMN2* substrate used contained the first 86 nucleotides of intron 7, including the 5′ ss, ISS-N1, URC1, URC2, and URC3. Mutant transcripts carried deletions/substitutions identical to the ones in the *SMN2* mutant minigenes used for the *in vivo* splicing assay (Fig. 5 and 7). The *in vitro* binding affinity of TIA1 to various RNA substrates was determined using the nitrocellulose-filter binding assay as described earlier (55). Our experimental design allowed comparison of binding strengths of two substrates in a single reaction. We performed two sets of

experiments. In the first set of experiments, all mutant transcripts were smaller than the wild-type transcript (Fig. 7B, lanes 1 to 20). Loadings were adjusted to maintain the wild-type construct at similar intensities in both input and bound fractions (Fig. 7B, top bands in lanes 1 to 20). Such an arrangement allowed easy comparison between input and bound fractions. In the second set of experiment, all mutant transcripts were the same size as the wild-type transcript (Fig. 7B, lanes 21 to 36). The binding strength of the mutants was compared with sequence 1-1, a 71-nucleotide-long RNA transcript that was shown to have high affinity for TIA1 (16). Here, loadings were adjusted to maintain sequence 1-1 at similar intensities in both input and bound fractions (Fig. 7B, bottom bands in lanes 21 to 36). Again, such an arrangement made a comparison between input and bound fractions easy.

In keeping with the preference of TIA1 for U-rich motifs, all deletions encompassing U residues had an adverse effect on TIA1 binding (Fig. 7). Among the 10 overlapping deletions tested, the individual or combined deletions of URC1 or URC2 were the most deleterious for TIA1 binding. The combined deletion of URC1 and URC2 led to a more than 6-fold decrease in TIA1 binding (Fig. 7, mutant I7Δ29-60), while the deletion encompassing URC3 that harbors the longest U-rich tract led to only a 2-fold decrease in TIA1 binding (Fig. 7, mutant I7Δ70-82). Interestingly, the deletion of URC2, which brings two U-rich sequences, URC1 and URC3, closer to each other, had a negative effect on TIA1 binding. These results indicate that the relative arrangement of URC1 and URC2 within wild-type context creates a high-affinity binding site for TIA1. Validating the results of deletion mutations, up to a 4-fold decrease in binding was observed for RNA transcripts bearing substitutions in URC1 or URC2 (Fig. 7). This observation indicates that the decreased binding of TIA1 to transcripts with deletions was due not merely to the reduction in their sizes. Overall, our results are consistent with a sequence-specific effect of TIA1-associated stimulation of *SMN2* exon 7 inclusion *in vivo* (Fig. 5). Interestingly, we observed that TIA1 showed higher affinity for wild-type *SMN2* RNA than sequence 1-1. This observation is significant and provides additional support in favor of a tight interaction between TIA1 and *SMN2* sequences downstream of ISS-N1. Notably, one of the mutants, URC1S2A, also showed high TIA1 binding despite the fact that this mutation in the *SMN2* minigene reduced the ability of overexpressed TIA1 to promote exon 7 inclusion. A discrepancy of this nature is not totally unexpected and could be attributed to a variety of factors, including creation of a binding site for a negative regulator of splicing. In general, the results of *in vitro* binding provide very strong evidence in support of a direct and sequence-specific interaction between TIA1 and the sequences downstream of ISS-N1.

Role of different domains in TIA1-mediated splicing regulation. There has been limited study on the role of individual TIA1 domains on splicing regulation *in vivo*. Due to the changed context of the TIA1 interaction away from the 5′ ss, we next wished to determine what portion of TIA1 governs its ability to affect *SMN2* exon 7 splicing. For this, we generated 3XFLAG expression vectors of individual TIA1 domains as well as different combinations of two and three domains (Fig. 8A). These expression vectors were cotransfected with the *SMN2* minigene, and total RNA and cellular lysates for Western blotting were prepared at 24 h posttransfection. The results of Western blotting confirmed that all TIA1 variants were expressed to comparable levels, except RRM2 and Q, whose expression levels were very low (Fig. 8C). These results are in line with the varied stability levels of different domains. However, our meticulous design of domain combinations was able to probe the significance of every single domain in the absence of one or more domains. As shown in Fig. 8B, individual RRM domains had no effect on exon 7 splicing. It is likely that the inability of individual RRM domains to stimulate exon 7 splicing could be due to poor nuclear import. Indeed, it has been shown that RRM2 is involved in nuclear import while RRM3 is important for nuclear export of the protein (68). However, immunocytochemistry with our representative RRM1 construct showed uniform distribution between nucleus and cytoplasm, suggesting that the loss of the stimulatory response of RRM1 is not due to the lack of its nuclear import (see Fig. S5 in the supplemental material).

The Q domain, despite its poor expression, caused a small but reproducible increase in exon 7 inclusion. This could be due to the inherent ability of the Q domain to interact with other proteins including endogenous TIA1/TIAR that may have been recruited, albeit poorly, at URC1/URC2. When the Q domain was added to any of the RRMs, the ability of these constructs to enhance exon 7 inclusion increased significantly, with RRM2+Q being the most and RRM3+Q being the least "splicing"-active variant (Fig. 8B). Remarkably, even with low expression, RRM2+Q was as effective as full-length TIA1 in promoting exon 7 inclusion. Other constructs in which the Q domain was absent produced very little, if any, effect on exon 7 splicing, except for RRM1+RRM2, which caused a small improvement in exon 7 inclusion (Fig. 8B, lanes 13 to 16). Constructs in which a single RRM domain was deleted were still able to promote exon 7 inclusion in the following order from most to least active: ΔRRM3, ΔRRM2, and ΔRRM1 (Fig. 8B, lanes 10 to 12). Taken together, our results suggest that the Q domain is indispensable for the ability of TIA1 to affect *SMN2* exon 7 splicing *in vivo*.

Distribution of splicing-stimulatory signals within the Q domain of TIA1. The TIA1 Q domain contains 21 glutamine residues unevenly distributed within a span of 97 amino acids located toward the C terminus of the protein. To evaluate the role of subsequences within the Q domain, we examined the effect of progressive deletions from the C terminus of TIA1 on *SMN2* exon 7 splicing. As shown in Fig. 9, deletion of the last 57 amino acids of TIA1 containing 10 glutamine residues had no effect on splicing (TIA1ΔQ3). However, further deletion of 20 additional amino acids led to a drastic decrease in the stimulatory effect of TIA1 (Fig. 9B, compare splicing patterns in the presence of TIA1ΔQ3 and TIA1ΔQ4). The stimulatory effect of TIA1 was almost entirely lost when the whole Q domain was deleted (Fig. 9, TIA1ΔQ5b). To eliminate the possibility that the lack of the Q domain negatively affected folding and therefore splicing activity of the TIA1, we generated fusion constructs in which ~30 unrelated amino acids were added to the C terminus of RRM1+2+3 (Fig. 8), generating the fusion 1a and fusion 2b constructs (Fig. 9A). Note that overexpression of RRM1+2+3 did not affect *SMN2* exon 7 splicing (Fig. 8B). Although the lengths of fusion 1a and 2b are comparable to the length of the relatively active TIA1ΔQ3

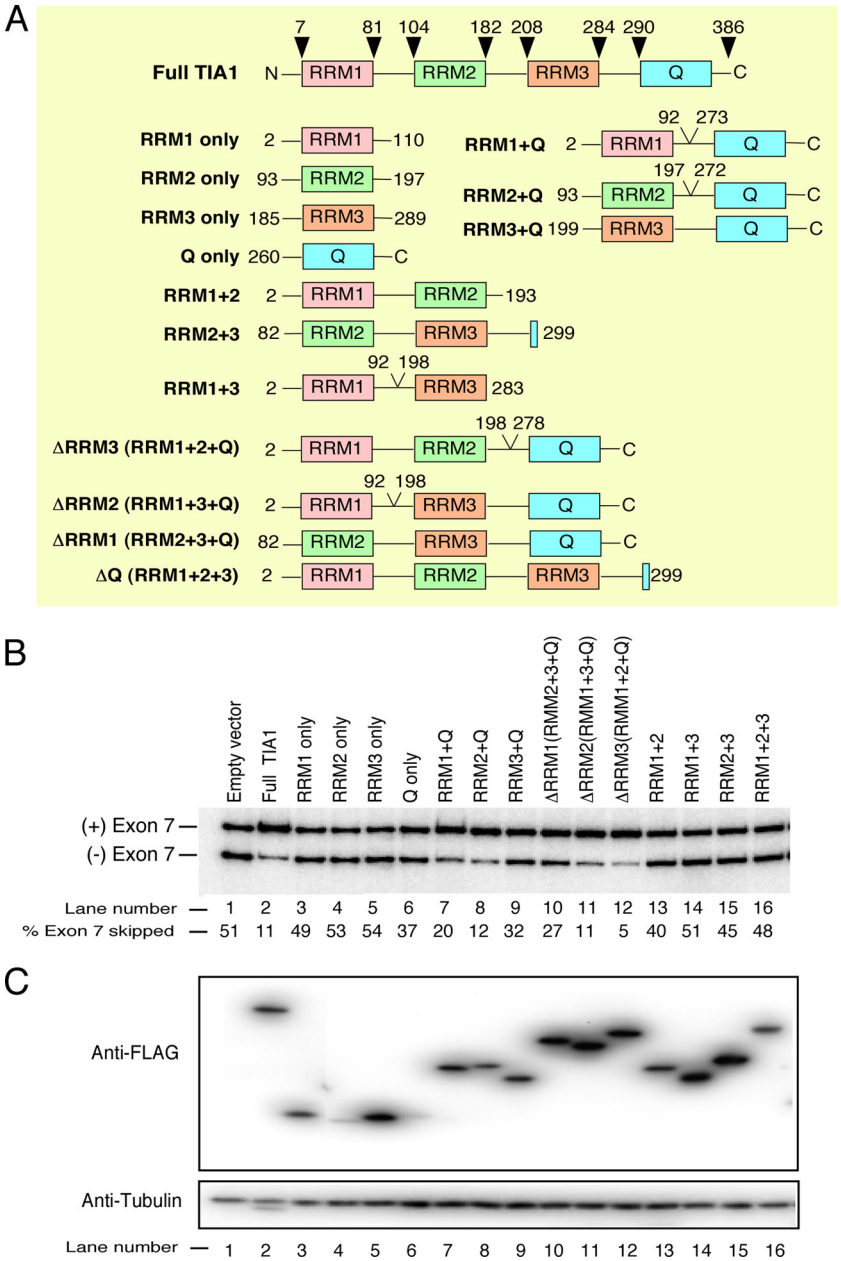

FIG. 8. Effect of different domains of TIA1 on *SMN2* exon 7 splicing. (A) Diagrammatic representation of the structure of full-length TIA1 and its derivative constructs. RRMs and the Q-rich domain are indicated. Numbers represent amino acid positions. Numbers in the full-length TIA1 were assigned based on Gilks et al. and Tian et al. (20, 57). (B) *In vivo* splicing pattern of the *SMN2* minigene in the presence of different TIA1 variants shown in panel A. All expressed TIA1 variants carried 3XFLAG tags at their N termini. HeLa cells were cotransfected with 0.04 μg of *SMN2* and either an empty vector or a TIA1 variant of interest. Amounts of expression vectors were adjusted to produce comparable levels of protein expression (see panel C) and varied from 0.4 μg to 1.96 μg. The total amount of DNA used per transfection was maintained constant by adding an empty vector when needed. Cells were collected 24 h after transfection. Results were analyzed as described in the legend of Fig. 1B. (C) Western blot confirming expression levels of TIA1 variants shown in panel A. Twenty micrograms of total protein was used for each sample. Equal protein loading was confirmed by reprobing the blot for α-tubulin. Primary antibodies used for probing are indicated on the left.

construct, neither fusion 1a nor fusion 2b showed appreciable improvement in promoting exon 7 inclusion (Fig. 9). Interestingly, fusion 2b had about twice as many glutamine residues as the wild-type subsequence and yet was unable to recover the stimulatory response. These results suggest that other residues in combination with glutamines may be contributing to the stimulatory effect of the Q domain on splicing.

Nuclear import of TIA1 is essential for its ability to affect pre-mRNA splicing. One *in vivo* study suggested that the first 50 amino acids of the Q domain of TIA1 are required for nuclear accumulation of TIA1 (68). On the other hand, an earlier *in vitro* study had implicated the Q domain in the recruitment of U1 snRNP at the 5′ ss (18). Our finding that the first half of the Q domain retains full stimulatory effect *in vivo*

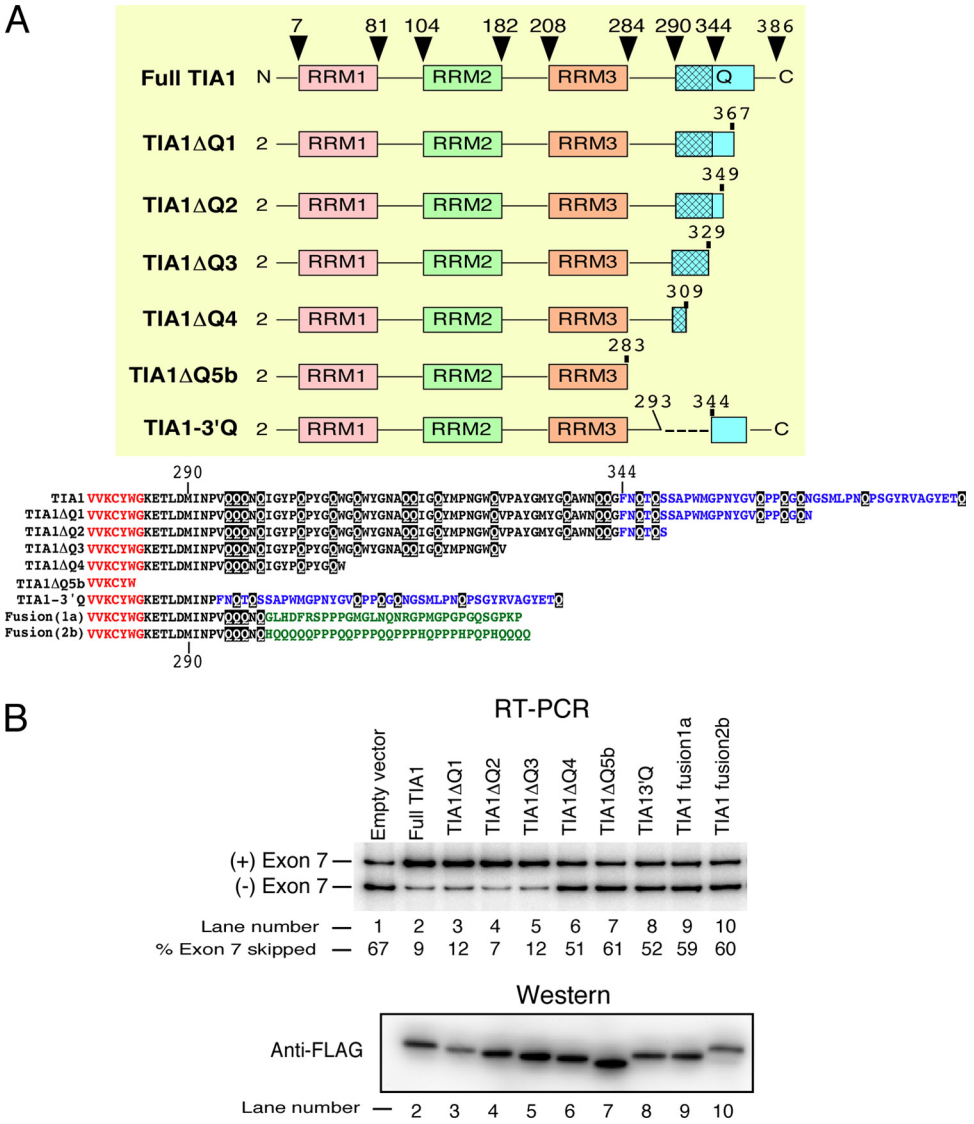

FIG. 9. Effect of Q-rich domain shortening on *SMN2* exon 7 splicing. (A) Diagrammatic representation of deletions/substitutions in the Q-rich domain of TIA1. RRMs and the Q-rich domain are indicated. Numbers represent amino acid positions. For the purposes of comparison, amino acid sequences of different deleted variants of the Q domain are given in the lower panel. Red letters represent C-terminal residues of RRM3. Black and blue letters denote the first 54 residues of the Q domain and the last 43 residues of TIA1, respectively. Green letters represent unrelated amino acid sequences added to the C terminus of a truncated TIA1 lacking the last 87 residues. Glutamine residues of TIA1 are shown in white letters and highlighted in black. (B) *In vivo* splicing pattern of the *SMN2* minigene in the presence of TIA1 proteins shown in panel A. All expressed TIA1 variants carried 3XFLAG tags at their N termini. HeLa cells were cotransfected with 0.04 μg of *SMN2* and either an empty vector or the TIA1 protein expression vector of interest. The amounts of TIA1 expression vectors were adjusted to produce comparable levels of protein expression (Western blot panel) and varied from 0.4 μg to 0.96 μg. The total amount of DNA used per transfection was maintained constant by the addition of empty vector when needed. Cells were collected for analysis 24 h after transfection as described in the legend of Fig. 8B and C.

is consistent with both observations. We next examined the impact of subsequences located in the second half of the Q domain. For this, we generated a TIA1 mutant in which the N-terminal portion of the Q domain from amino acid 294 to amino acid 343 was deleted (Fig. 9A, TIA1-3′Q). Interestingly, this variant regained some stimulatory response on splicing compared to the TIA1ΔQ5b construct in which the entire 97 residues of the Q domain were deleted (Fig. 9B). These results reveal that the second half of the Q domain, despite its low Q content, retains some of the stimulatory function.

TIA1 counteracts the inhibitory effect of PTB. The multifunctional PTB (also referred to as hnRNP I) is a widely expressed protein that binds preferentially to polypyrimidine-rich sequences (2, 45, 46, 54). PTB contains four RRMs and an N-terminal nuclear localization signal. Nuclear magnetic resonance (NMR) structures of PTB RRMs show variations in sequence preferences (2). In addition to interaction with pyrimidine-rich sequences, three RRMs (RRM2, RRM3, and RRM4) of PTB are capable of engaging in protein-protein interactions (2). PTB is known to facilitate exon skipping by

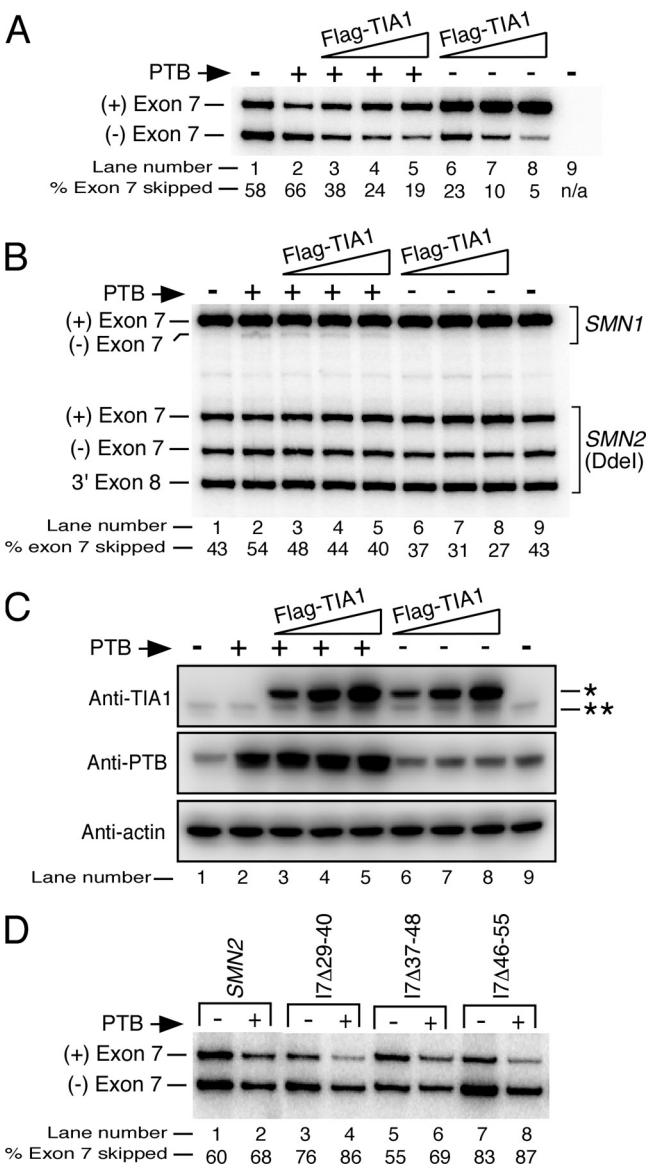

FIG. 10. (A) *In vivo* splicing pattern of the *SMN2* minigene in the presence of overexpressed PTB1 and TIA1. HeLa cells grown in six-well plates were cotransfected with 0.04 μg of *SMN2* (lanes 1 to 8), 0.3 μg of myc-PTB expression vector (lanes 2 to 5), and various amounts of 3XFLAG-hTIA1 (0. 36 μg in lanes 3 and 6; 0. 73 μg in lanes 4 and 7; and 1.46 μg in lanes 5 and 8). Lane 9 served as an untransfected control. The total amount of DNA used per transfection was maintained constant by the addition of empty vector when needed. Cells were collected 24 h after transfection. Results were analyzed as described in the legend of Fig. 1B. (B) Effect of overexpressed PTB and TIA1 on splicing of endogenous *SMN* exon 7. Cotransfections were done as described in panel A. Spliced products were analyzed by RT-PCR as described in panel A, except that different primers, one located in exon 6 (N-24) and the other in the portion of exon 8 that is absent in the minigene (P26), were used. Following RT-PCR, DdeI digestion was performed to distinguish spliced products from *SMN2* (35). The percentage of *SMN2* exon 7 skipping was calculated as described in the legend of Fig. 1D. (C) Western blot showing the levels of endogenous and recombinant myc-tagged PTB as well as endogenous and recombinant FLAG-tagged TIA1. Twenty micrograms of total protein was used for each sample. Equal protein loading was confirmed by reprobing the blot for β-actin. Primary antibodies used for probing are indicated on the left. Bands corresponding to FLAG-tagged (*) and endogenous (**) TIA1 are marked on the right. (D) Effect of URC1 and URC2 deletions on the ability of PTB to promote *SMN2* exon 7 skipping. HeLa cells grown in 24-well plates were cotransfected with 0.04 μg of a given minigene and 0.30 μg of either empty vector or myc-PTB. Mutants are described the legend of Fig. 5A. Total RNA was isolated 24 h posttransfection. Results were analyzed as described in the legend of Fig. 1B

preventing recruitment of U2AF at the branch point, which is located within the polypyrimidine tract immediately upstream of an exon (54). Other skipping mechanisms take advantage of multiple interactions at different sites within pre-mRNA. Such interactions either loop out the exon or create a zone of silencing (30, 60). Recently, PTB has been found to bind to element 1, a silencer within intron 6 of *SMN2* (4). However, the mechanism by which PTB affects *SMN* exon 7 splicing remains unknown. It is likely that *SMN2* exon 7 splicing is regulated by a combinatorial control in which the inhibitory effect of PTB is offset, at least in part, by the stimulatory effect of TIA1. To explore such a possibility, we set out to compare the splicing patterns of the *SMN2* minigene in HeLa cells overexpressing PTB and/or 3XFLAG-hTIA1. We began our experiments with optimization of PTB expression. Moderate expression of myc-tagged PTB from 0.30 μg of PTB expression vector produced a noticeable increase in *SMN2* exon 7 skipping (Fig. 10A and C). Of note, a further increase in the amount of this vector used for transfection led to a substantial drop in the levels of *SMN* transcripts (data not shown). This could be due to an indirect effect owing to alternation of other cellular processes (46). To check the stimulatory response of TIA1, we employed various concentrations of the TIA1 expression vector starting from 0.36 μg. Expression levels of both PTB and TIA1 were confirmed by Western blotting (Fig. 10C). Our lowest TIA1 expression was able to fully counteract the inhibitory effect of PTB while the highest TIA1 expression not only nullified the inhibitory effect of PTB but also substantially restored exon 7 inclusion in transcripts derived from the *SMN2* minigene (Fig. 10A). We then compared the splicing pattern of endogenous *SMN* exon 7 in the above samples employing a primer combination that does not amplify minigene transcripts. PTB caused increased skipping from 43% to 54% (Fig. 10B). A high concentration of TIA1 was able to counteract the inhibitory effect of PTB and fully restored *SMN2* exon 7 inclusion to the level observed in untransfected cells (Fig. 10B). Interestingly, overexpressed PTB had a mild inhibitory effect on endogenous *SMN1* exon 7 splicing. Here again, a high concentration of TIA1 was able to counteract this effect (Fig. 10B).

To test whether PTB-associated skipping of *SMN2* exon 7 is executed through URC1 and URC2, polypyrimidine-rich sequences responsible for interaction with TIA1, we took advantage of some of our previously described mutants. We compared the splicing patterns of these mutants with or without overexpressed PTB. Deletion of URC1 (mutant I7Δ29–40) or URC2 (mutant I7Δ46–55) or sequences between URC1 and URC2 (mutant I7Δ37–48) did not affect the ability of PTB to promote *SMN2* exon 7 skipping (Fig. 10D). These results suggest that the TIA1 binding site within intron 7 does not overlap with the motif responsible for PTB interaction. Interestingly,

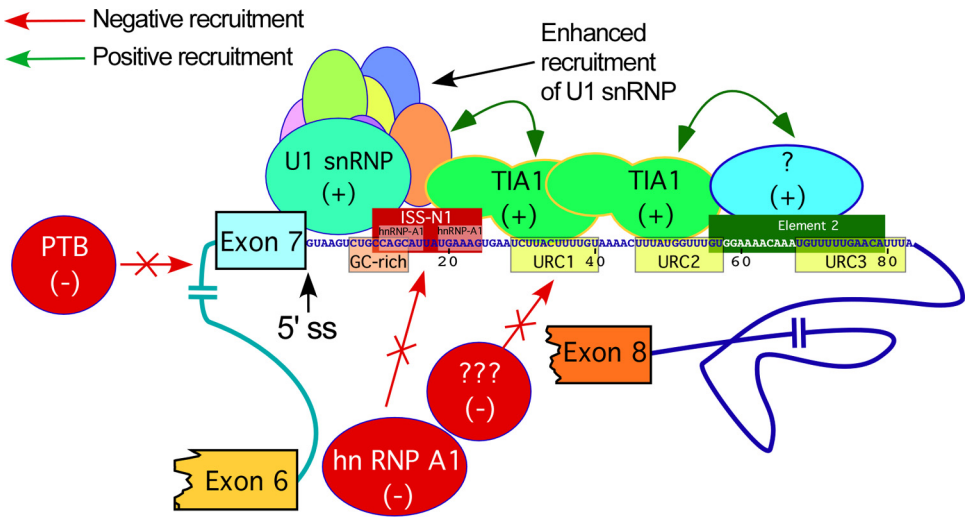

FIG. 11. Model of TIA1-mediated splicing regulation of *SMN2* exon 7 splicing. The 5′ portion of *SMN* intron 7 sequence containing various splicing *cis* elements is shown. Numbering of nucleotides starts from the first position of intron 7. Roles of intronic *cis* elements ISS-N1, GC-rich, element 2, and hnRNP A1 and PTB motifs have been described previously (4, 24, 41, 48, 52). Plus and minus signs indicate that a given splicing factor promotes exon 7 inclusion and skipping, respectively. The nature of the stimulatory factor(s) (represented by "?") interacting with element 2 is not known. Binding of TIA1 to URC1/URC2 brings a change in the context leading to recruitment of U1 snRNP at the 5′ ss of exon 7. Also, a TIA1-associated change in the context creates an unfavorable condition for the recruitment of negative splicing factors including hnRNP A1 and PTB.

these findings are consistent with the absence of a UYUYU subsequence within URC1 or URC2. This subsequence was recently identified as the top consensus motif for a PTB-RNA interaction in a genome-wide analysis *in vivo* (64). Our results support the role of TIA1 in counteracting the negative impact of PTB on *SMN* exon 7 splicing.

DISCUSSION

Recent reports reveal critical roles for TIA1 and TIAR in genome-wide positive regulation of pre-mRNA splicing through specific interactions involving U-rich intronic motifs adjacent to the 5′ ss of exons (3, 19). The close proximity of intronic U-rich sequences to the 5′ ss allows TIA1 to facilitate 5′ ss recognition by recruitment of U1 snRNP through direct interactions (9, 15, 18, 32). Such a mechanism may exclude a role for TIA1 in different contexts in which U-rich intronic motifs are separated from the 5′ ss by intervening negative intronic *cis* elements. Moreover, it is not known if the stimulatory role of TIA1 is at all applicable to contexts in which U-rich intronic motifs are located more than 30 nucleotides away from the 5′ ss. To explore the role of TIA1 in such a context, we took advantage of *SMN2* exon 7, skipping of which is associated with SMA, a leading neurodegenerative disease. The intronic sequences immediately downstream of the 5′ ss of exon 7 are marked by the absence of U-rich motifs characteristic of TIA1 binding sites. In addition, the first 24 residues of intron 7 harbor overlapping inhibitory *cis* elements (24, 48, 52, 53) (Fig. 11). Here, we report that TIA1 plays a prominent stimulatory role in *SMN2* exon 7 splicing through novel intronic motifs located away from the 5′ ss.

A significant effect of TIA1 on *SMN2* exon 7 splicing regulation emerged from a series of complementary experiments that we performed *in vivo*. First, overexpression of recombinant TIA1 or its closely related analog, TIAR, led to a substantial increase in exon 7 inclusion in transcripts derived from the *SMN2* minigene. A stimulatory effect of TIA1 was also observed on exon 7 splicing from endogenous *SMN2*. Supporting the result of TIA1 overexpression, *SMN* minigenes transfected in a TIA1 knockout mouse cell line ($TIA1^{-/-}$ cells) showed increased skipping of exon 7. The negative consequence of the absence of TIA1 was specific to human *SMN* as splicing of mouse *Smn* exon 7 appeared unaffected in $TIA1^{-/-}$ cells. Further validating the positive role of TIA1 and TIAR on *SMN2* exon 7 splicing, depletion of these factors using an siRNA-based approach led to an increase in *SMN2* exon 7 skipping.

To determine the role of a specific sequence(s) responsible for a TIA1-associated stimulatory effect on *SMN2* exon 7 splicing, we adopted an open-ended approach in which we first scanned the entire intron 7 through large deletions. With our largest deletion (I7Δ190–406), which eliminated numerous URCs, including the longest U-rich motif comprised of eight U residues in the 3′-half of intron 7, the stimulatory effect of TIA1 was fully retained. These results ruled out the possibility that the TIA1 binding site is located in the 3′ half of intron 7. Thus, we focused on sequences in the first half of intron 7. Overlapping deletions in this region revealed URC1 (UCUU ACUUUUGU) and URC2 (UUUAUGGUUUGU) as possible sites of TIA1 interaction. URC1 and URC2 fall within 29th and 57th positions of intron 7. Of note, simultaneous deletion of URC1 and URC2 led to a complete loss of the TIA1-associated stimulatory effect despite the fact that this deletion brought URC3 (UGUUUUUGAACAUUUA) closer to the 5′ ss. Complementing the results of deletion mutations, ASOs blocking URC1 and URC2 led to increased *SMN2* exon 7 skipping, even in the presence of overexpressed TIA1. The results of ASO-based experiments were significant in ruling out

the possibility of an indirect effect of inhibitory elements that may have been inadvertently created by deletion mutations. Further supporting the URC1/URC2-dependent stimulatory role of TIA1, overexpression of TIA1 led to an increase in exon inclusion in a heterologous context. Portability of URC1/URC2 in a heterologous context underscores that TIA1/TIAR may have an expanded role in splicing regulation through URC1/URC2-like motifs away from the 5′ ss.

To accurately define the TIA1 binding site, we used small overlapping deletions. Several of these short deletions that either fully or partially eliminated URC1 and/or URC2 reduced the stimulatory effect of TIA1. These results imply roles for both URC1 and URC2 in TIA1 binding. Complementing the results of deletion mutations, substitutions within URC1 and URC2 also led to a decrease in/loss of the stimulatory effect of TIA1. To confirm that *in vivo* splicing results of *SMN2* minigenes containing deletion and substitution mutations are in concert with the loss of a direct interaction of TIA1 with URC1 and URC2, we performed *in vitro* binding using purified TIA1 and transcripts harboring identical mutations. The results of *in vitro* binding fully supported a direct interaction of TIA1 with URC1 and URC2. Consistently, substitutions within URC1 or URC2 led to a reduction in affinity of TIA1 for RNA. Results of *in vitro* binding also revealed that the interaction between URC1/URC2 and TIA1 is tighter than the interaction of TIA1 with a high-affinity TIA1 binder isolated using *in vitro* selection (Fig. 7). These results underscore that very low levels of TIA1 in the nucleus should be able to modulate *SMN2* exon 7 splicing.

Having determined the sequence-specific effect of TIA1 in a novel context, we next examined the impact of individual TIA1 domains on *SMN2* exon 7 splicing. Our results revealed the essential role of the Q domain and confirmed that any RRM in combination with the Q domain is necessary and sufficient to stimulate *SMN2* exon 7 splicing *in vivo*. This is not totally unexpected since the RRMs of TIA1 share a high degree of homology (57). Of note, a positive effect of a given TIA1 domain combination on pre-mRNA splicing *in vivo* is dependent upon several limiting events, including a relatively moderate expression, an appreciable level of nuclear import, a reasonable affinity for the target, and the ability of this domain combination to favorably interact with components of spliceosome. Our finding that any RRM in combination with the Q domain is able to stimulate *SMN2* exon 7 splicing is distinct from an *in vitro* study showing a specific requirement for RRM1 in addition to the Q domain for the formation of a tight interaction with U1 snRNP (18). The discrepancy between *in vivo* and *in vitro* results could be due to several factors, including a change in the context of the 5′ ss and coupling of pre-mRNA splicing with transcription and polyadenylation *in vivo*. A previous localization study had suggested a requirement for RRM2 and RRM3 in nuclear import and export, respectively (68). However, since the study did not employ a nuclear function in a sufficiently sensitive assay, the significance of reduced nuclear import or export of a particular domain combination could not be evaluated. Our finding that the lack of RRM2 has no adverse effect on *SMN2* exon 7 splicing suggests that RRM2 might be dispensable for nuclear import. Our results argue that even a suboptimal level of nuclear import of a critical splicing factor may have a substantial impact on pre-mRNA splicing. In agreement with the results of different domain combinations of TIA1, overexpression of TIA1Δ5 and TIARΔ3 increased *SMN2* exon 7 inclusion. These two proteins are the major spliced variants of TIA1 and TIAR, respectively. Based on our findings, we believe that even shorter and less frequent spliced variants of TIA1 and TIAR would be able to stimulate *SMN2* exon 7 inclusion.

The essential role of the Q domain in *SMN2* exon 7 splicing prompted us to examine this domain in further detail. Unlike the characteristic two RNP motifs within each RRM, the Q domain does not contain a signature motif. Twenty-one glutamine residues are randomly distributed within the Q domain. With a deletion of the last half of the Q domain, most of the splicing activity was retained, and some splicing activity was retained with deletion of the first half of the Q domain. These results suggest a cumulative effect in which a large number of glutamine residues in the first half of the Q domain contributed toward the maximum activity. Consistently, the first 19 amino acids of the Q domain contain the highest density of glutamine residues (~32%) as well as the longest Q-rich motif (QQQNQ), and this region was able to retain about one-third of the total activity. These results, however, do not rule out the possibility that amino acids other than glutamine residues in the Q domain might play a supportive role in the splicing-associated function of TIA1.

Our results support the bipartite nature of an interaction in which TIA1 contacts two motifs (URC1 and URC2) within a span of 29 nucleotides between the 29th and 57th positions of intron 7. Such an interaction is consistent with the structural studies in which the interface between RNA and an interacting RRM domain is generally occupied by less than seven nucleotides (11). In the case of TIA1, the bipartite nature of interaction is possible through two RRMs of either the same or different TIA1 molecules. Our finding that a single RRM in combination with the Q domain is able to stimulate exon 7 inclusion suggests that URC1/URC2 is bound by a TIA1 dimer. In addition, the high affinity of TIA1 to URC1/URC2 fits well with the dimeric mode of interactions in which protein binding to RNA is stabilized by protein-protein interactions and vice versa.

Different mechanisms may account for the stimulation of *SMN2* exon 7 inclusion by TIA1. The most plausible among those is the "prevention of negative recruitment." According to this model, TIA1 interaction with URC1/URC2 prevents recruitment of negative factors, including hnRNP A1, upstream of the TIA1 binding site (Fig. 11). This, in turn, would lead to enhanced recruitment of U1 snRNP due to a now accessible 5′ ss. This hypothesis is consistent with complementary findings in which ASO-mediated blocking of a GC-rich motif or ISS-N1 promotes *SMN2* exon 7 inclusion (24, 48, 52). In addition, our recent report revealed a long-distance negative interaction involving the 10th intronic position (53). Binding of TIA1 to URC1/URC2 has a potential to prevent/abrogate this negative interaction through hindering and/or sterically impacting the accessibility of the 10th intronic position. The hypothesis of the prevention of negative recruitment does not exclude another possibility, i.e., that URC1/URC2-bound TIA1 directly recruits U1 snRNP through looping out sequences between the 5′ ss and the TIA1 binding site. This hypothesis is consistent with

the ability of RRMs and the Q domain to participate in protein-protein interactions (11).

Notable finding that TIA1 is able to counteract the inhibitory effect of PTB suggests additional mechanisms in which recruitment of TIA1 to URC1/URC2 brings dramatic changes in the context of pre-mRNA. PTB promotes exon skipping through different mechanisms (2). The most common among them is the looping out of the skipped exon through binding to flanking intronic sequences (30). A recent genome-wide analysis revealed subsequence UYUYU as the top scored consensus motif for PTB-RNA interactions *in vivo* (64). Intronic sequences flanking *SMN* exon 7 are replete with such sequences. Also, PTB has been shown to interact with element 1, which is located within intron 6 of *SMN* (4). Element 1 harbors subsequence UUUUU as one of the top-scored PTB binding motifs. Consistent with the absence of a UYUYU motif, our functional study ruled out the presence of a PTB binding site within URC1/URC2, which is the site of interaction with TIA1. However, there are additional UYUYU motifs downstream of URC1/URC2. Interaction of PTB with element 1 within *SMN* intron 6 and possible interaction within intron 7 may support the looping-out mechanism. Another mechanism of PTB-associated splicing regulation supports the formation of a zone of silencing around a skipped exon (60). In addition to PTB, other inhibitory factors such as hnRNP A1 and Sam68 have been implicated in promotion of *SMN2* exon 7 skipping. It is possible that PTB forms a zone of silencing around *SMN2* exon 7 through interactions involving additional negative factors including, but not limited to, hnRNP A1 and Sam68. Our results suggest that the TIA1-induced contextual change within *SMN* pre-mRNA is sufficient to prevent the inhibitory effect of PTB on *SMN* exon 7 splicing.

SMN is a multifunctional protein with more than 20 reported interacting partners. Through regulation of snRNP biogenesis in the nucleus, SMN controls the rate of pre-mRNA splicing. Consistently, depletion of SMN leads to genome-wide perturbations of pre-mRNA splicing (70). SMN is a component of stress granules, a dynamic cytoplasmic structure, formation of which requires TIA1 and hnRNP A1 (22, 25). hnRNP A1 is a negative regulator of *SMN2* exon 7 splicing. Two out of four putative hnRNP A1 binding sites are located immediately upstream of the TIA1 binding site within intron 7. Our discovery of TIA1 as a regulator of *SMN* exon 7 splicing provides a unique precedence in which two splicing factors (TIA1 and hnRNP A1) that cooperate in response to cellular stress play opposing roles in regulation of *SMN2* exon 7 splicing through adjacent intronic motifs located in the vicinity of the 5′ ss. Thus far, studies on TIA1-assisted pre-mRNA splicing regulation have focused on U-rich motifs close to the 5′ ss. The finding that TIA1 could modulate exon 7 inclusion through U-rich intronic motifs separated from the 5′ ss by negative *cis* elements brings new insight into our understanding of pre-mRNA splicing of a critical exon associated with SMA, a leading genetic disease of children and infants. Reduced levels of SMN in SMA primarily affect motor neurons that generally maintain high levels of SMN. It is also known that TIA1, TIAR, and PTB are abundantly expressed in the brain (5, 14). Hence, regulation *SMN2* exon 7 splicing by TIA1/TIAR has significance in maintaining the high levels of SMN in the brain. Skipping of *SMN2* exon 7 has been also associated with conditions of oxidative stress that causes Parkinson's and Alzheimer's disease (37). Thus, our findings provide a broader role of TIA1/TIAR in alleviating the severity of a large number of diseases associated with low levels of SMN.

ACKNOWLEDGMENTS

We express our gratitude to Paul Anderson for providing the mouse TIA1$^{-/-}$ cell line and Douglas Black for providing the myc-tagged PTB expression vector. We acknowledge technical support provided by Sarah J. Rahn and Katrin Hollinger.

This work was supported by a grant from U.S. National Institutes of Health (R01NS055925) to R.N.S. R.N.S. acknowledges support of Salsbury Endowment at Iowa State University, Ames, IA. N.N.S. was supported by grants from the Center for Integrated Animal Genomics and Iowa Center for Advance Neurotoxicology.

REFERENCES

1. **Anderson, P., and N. Kedersha.** 2009. RNA granules: post-transcriptional and epigenetic modulators of gene expression. Nat. Rev. Mol. Cell Biol. **10:**430–436.
2. **Auweter, S. D., and F. H. Allain.** 2008. Structure-function relationships of the polypyrimidine tract binding protein. Cell. Mol. Life Sci. **65:**516–527.
3. **Aznarez, I., et al.** 2008. A systematic analysis of intronic sequences downstream of 5′ splice sites reveals a widespread role for U-rich motifs and TIA1/TIAL1 proteins in alternative splicing regulation. Genome Res. **18:** 1247–1258.
4. **Baughan, T. D., A. Dickson, E. Y. Osman, and C. L. Lorson.** 2009. Delivery of bifunctional RNAs that target an intronic repressor and increase SMN levels in an animal model of spinal muscular atrophy. Hum. Mol. Genet. **18:**1600–1611.
5. **Beck, A. R., Q. G. Medley, S. O'Brien, P. Anderson, and M. Streuli.** 1996. Structure, tissue distribution and genomic organization of the murine RRM-type RNA binding proteins TIA-1 and TIAR. Nucleic Acids Res. **24:**3829–3835.
6. **Chasin, L. A.** 2007. Searching for splicing motifs. Adv. Exp. Med. Biol. **623:**85–106.
7. **Chen, H. H., J. G. Chang, R. M. Lu, T. Y. Peng, and W. Y. Tarn.** 2008. The RNA binding protein hnRNP Q modulates the utilization of exon 7 in the *survival motor neuron* 2 (*SMN2*) gene. Mol. Cell. Biol. **28:**6929–6938.
8. **Cho, S., and G. Dreyfuss.** 2010. A degron created by SMN2 exon 7 skipping is a principal contributor to spinal muscular atrophy severity. Genes Dev. **24:**438–442.
9. **Choi, E. Y., and D. Pintel.** 2009. Splicing of the large intron present in the nonstructural gene of minute virus of mice is governed by TIA-1/TIAR binding downstream of the nonconsensus donor. J. Virol. **83:**6306–6311.
10. **Chong, S. R., et al.** 1997. Single-column purification of free recombinant proteins using a self-cleavable affinity tag derived from a protein splicing element. Gene **192:**271–281.
11. **Cléry, A., M. Blatter, and F. H. Allain.** 2008. RNA recognition motifs: boring? Not quite. Curr. Opin. Struct. Biol. **18:**290–298.
12. **Cooper, T. A., L. Wan, and G. Dreyfuss.** 2009. RNA and disease. Cell **136:**777–793.
13. **David, C. J., and J. L. Manley.** 2008. The search for alternative splicing regulators: new approaches offer a path to a splicing code. Genes Dev. **22:**279–285.
14. **de la Grange, P., L. Gratadou, M. Delord, M. Dutertre, and D. Auboeuf.** 2010. Splicing factor and exon profiling across human tissues. Nucleic Acids Res. **38:**2825–2838.
15. **Del Gatto-Konczak, F., et al.** 2000. The RNA-binding protein TIA-1 is a novel mammalian splicing regulator acting through intron sequences adjacent to a 5′ splice site. Mol. Cell. Biol. **20:**6287–6299.
16. **Dember, L. M., N. D. Kim, K. Q. Liu, and P. Anderson.** 1996. Individual RNA recognition motifs of TIA-1 and TIAR have different RNA binding specificities. J. Biol. Chem. **271:**2783–2788.
17. **Fisette, J. F., J. Toutant, S. Dugré-Brisson, L. Desgroseillers, and B. Chabot.** 2010. hnRNP A1 and hnRNP H can collaborate to modulate 5′ splice site selection. RNA **16:**228–238.
18. **Förch, P., O. Puig, C. Martinez, B. Seraphin, and J. Valcarcel.** 2002. The splicing regulator TIA1 interacts with U1-C to promote U1 snRNP recruitment to 5′ splice sites. EMBO J. **21:**6882–6892.
19. **Gal-Mark, N., S. Schwartz, O. Ram, E. Eyras, and G. Ast.** 2009. The pivotal roles of TIA proteins in 5′ splice-site selection of alu exons and across evolution. PLoS Genet. **5:**e1000717.
20. **Gilks, N., et al.** 2004. Stress granule assembly is mediated by prion-like aggregation of TIA-1. Mol. Biol. Cell **15:**5383–5398.
21. **Gladman, J. T., and D. S. Chandler.** 2009. Intron 7 conserved sequence elements regulate the splicing of the SMN genes. Hum. Genet. **126:**833–841.
22. **Guil, S., J. C. Long, and J. F. Caceres.** 2006. hnRNP A1 relocalization to the

stress granules reflects a role in the stress response. Mol. Cell. Biol. **26:**5744–5758.
23. **Hofmann, Y., C. L. Lorson, S. Stamm, E. J. Androphy, and B. Wirth.** 2000. Htra2-beta stimulates an exonic splicing enhancer and can restore full-length SMN expression to survival motor neuron 2 (SMN2). Proc. Natl. Acad. Sci. U. S. A. **97:**9618–9623.
24. **Hua, Y., T. A. Vickers, H. L. Okunola, C. F. Bennett, and A. R. Krainer.** 2008. Antisense masking of an hnRNP A1/A2 intronic splicing silencer corrects SMN2 splicing in transgenic mice. Am. J. Hum. Genet. **82:**834–848.
25. **Hua, Y., and J. Zhou.** 2004. Survival motor neuron protein facilitates assembly of stress granules. FEBS Lett. **572:**69–74.
26. **Ibrahim, E. C., T. D. Schaal, K. J. Hertel, R. Reed, and T. Maniatis.** 2005. Serine/arginine-rich protein-dependent suppression of exon skipping by exonic splicing enhancers. Proc. Natl. Acad. Sci. U. S. A. **102:**5002–5007.
27. **Irimia, M., J. L. Rukov, and S. W. Roy.** 2009. Evolution of alternative splicing regulation: changes in predicted exonic splicing regulators are not associated with changes in alternative splicing levels in primates. PLoS One **4:**e5800.
28. **Izquierdo, J. M., and J. Valcárcel.** 2007. Two isoforms of the T-cell intracellular antigen 1 (TIA-1) splicing factor display distinct splicing regulation activities. Control of TIA-1 isoform ratio by TIA-1-related protein. J. Biol. Chem. **282:**19410–19417.
29. **Kawakami, A., et al.** 1992. Identification and functional characterization of a TIA-1-related nucleolysin. Proc. Natl. Acad. Sci. U. S. A. **89:**8681–8685.
30. **Lamichhane, R., et al.** 2010. RNA looping by PTB: evidence using FRET and NMR spectroscopy for a role in splicing repression. Proc. Natl. Acad. Sci. U. S. A. **107:**4105–4110.
31. **Lefebvre, S., et al.** 1997. Correlation between severity and SMN protein level in spinal muscular atrophy. Nat. Genet. **16:**265–269.
32. **Le Guiner, C., et al.** 2001. TIA-1 and TIAR activate splicing of alternative exons with weak 5′ splice sites followed by a U-rich stretch on their own pre-mRNA. J. Biol. Chem. **276:**40638–40646.
33. **Li, W., et al.** 2002. Cell proteins TIA-1 and TIAR interact with the 3′ stem-loop of the West Nile virus complementary minus-strand RNA and facilitate virus replication. J. Virol. **76:**11989–12000.
34. **Lin, S., and X. D. Fu.** 2007. SR proteins and related factors in alternative splicing. Adv. Exp. Med. Biol. **623:**107–122.
35. **Lorson, C. L., E. Hahnen, E. J. Androphy, and B. Wirth.** 1999. A single nucleotide in the SMN gene regulates splicing and is responsible for spinal muscular atrophy. Proc. Natl. Acad. Sci. U. S. A. **96:**6307–6311.
36. **Lorson, C. L., H. Rindt, and M. Shababi.** 2010. Spinal muscular atrophy: mechanisms and therapeutic strategies. Hum. Mol. Genet. **19:**R111–R118.
37. **Maracchioni, A., et al.** 2007. Mitochondrial damage modulates alternative splicing in neuronal cells: implication for neurodegeneration. J. Neurochem. **100:**142–153.
38. **Martins de Araújo, M., S. Bonnal, M. L. Hastings, A. R. Krainer, and J. Valcárcel.** 2009. Differential 3′ splice site recognition of SMN1 and SMN2 transcripts by U2AF and U2 snRNP. RNA **15:**515–523.
39. **Mende, Y., et al.** 2010. Deficiency of the splicing factor Sfrs10 results in early embryonic lethality in mice and has no impact on full-length SMN/Smn splicing. Hum. Mol. Genet. **19:**2154–2167.
40. **Mercado, P. A., Y. M. Ayala, M. Romano, E. Buratti, and F. E. Baralle.** 2005. Depletion of TDP 43 overrides the need for exonic and intronic splicing enhancers in the human apo-II gene. Nucleic Acids Res. **33:**6000–6010.
41. **Miyaso, H., et al.** 2003. An intronic splicing enhancer element in survival motor neuron (SMN) pre-mRNA. J. Biol. Chem. **278:**15825–15831.
42. **Nilsen, T. W., and B. R. Graveley.** 2010. Expansion of eukaryotic proteome by alternative splicing. Nature **463:**457–463.
43. **Pagani, F., et al.** 2003. New type of disease causing mutations: the example of the composite exonic regulatory elements of splicing in CFTR exon 12. Hum. Mol. Genet. **12:**1111–1120.
44. **Pedrotti, S., et al.** 2010. The splicing regulator Sam68 binds to a novel exonic splicing silencer and functions in SMN2 alternative splicing in spinal muscular atrophy. EMBO J. **29:**1235–1247.
45. **Perez, I., C. H. Lin, J. G. McAfee, and J. G. Patton.** 1997. Mutation of PTB binding sites causes misregulation of alternative 3′ splice site selection in vivo. RNA **3:**764–778.
46. **Sawicka, K., M. Bushell, K. A. Spriggs, and A. E. Willis.** 2008. Polypyrimidine-tract-binding protein: a multifunctional RNA-binding protein. Biochem. Soc. Trans. **36:**641–647.
47. **Shepard, P. J., and K. J. Hertel.** 2008. Conserved RNA secondary structures promote alternative splicing. RNA **14:**1463–1469.
48. **Singh, N. K., N. N. Singh, E. J. Androphy, and R. N. Singh.** 2006. Splicing of a critical exon of human survival motor neuron is regulated by a unique silencer element located in the last intron. Mol. Cell. Biol. **26:**1333–1346.
49. **Singh, N. N., E. J. Androphy, and R. N. Singh.** 2004. An extended inhibitory context causes skipping of exon 7 of SMN2 in spinal muscular atrophy. Biochem. Biophys. Res. Commun. **315:**381–388.
50. **Singh, N. N., E. J. Androphy, and R. N. Singh.** 2004. In vivo selection reveals combinatorial controls that define a critical exon in the spinal muscular atrophy genes. RNA **10:**1291–1305.
51. **Singh, N. N., R. N. Singh, and E. J. Androphy.** 2007. Modulating role of RNA structure in alternative splicing of a critical exon in the spinal muscular atrophy genes. Nucleic Acids Res. **35:**371–389.
52. **Singh, N. N., M. Shishimorova, L. C. Cao, L. Gangwani, and R. N. Singh.** 2009. A short antisense oligonucleotide masking a unique intronic motif prevents skipping of a critical exon in spinal muscular atrophy. RNA Biol. **6:**341–350.
53. **Singh, N. N., K. Hollinger, D. Bhattacharya, and R. N. Singh.** 2010. An antisense microwalk reveals critical role of an intronic position linked to a unique long-distance interaction in pre-mRNA splicing. RNA **16:**1167–1181.
54. **Singh, R., J. Valcarcel, and M. R. Green.** 1995. Distinct binding specificities and functions of higher eukaryotic polypyrimidine tract-binding proteins. Science **268:**1173–1176.
55. **Singh, R. N., R. J. Saldanha, L. M. D'Souza, and A. M. Lambowitz.** 2002. Binding of a group II intron-encoded reverse transcriptase/maturase to its high affinity intron RNA binding site involves sequence-specific recognition and autoregulates translation. J. Mol. Biol. **318:**287–303.
56. **Singh, R. N.** 2007. Evolving concepts on human SMN pre-mRNA splicing. RNA Biol. **4:**7–10.
57. **Tian, Q., M. Streuli, H. Saito, S. F. Schlossman, and P. Anderson.** 1991. A polyadenylate binding protein localized to the granules of cytolytic lymphocytes induces DNA fragmentation in target cells. Cell **67:**629–639.
58. **Vitte, J., et al.** 2007. Refined characterization of the expression and stability of the SMN gene products. Am. J. Pathol. **171:**1269–1280.
59. **Voelker, R. B., and J. A. Berglund.** 2007. A comprehensive computational characterization of conserved mammalian intronic sequences reveals conserved motifs associated with constitutive and alternative splicing. Genome Res. **17:**1023–1033.
60. **Wagner, E. J., and M. A. Garcia-Blanco.** 2001. Polypyrimidine tract binding protein antagonizes exon definition. Mol. Cell. Biol. **21:**3281–3288.
61. **Wang, Z., and C. B. Burge.** 2008. Splicing regulation: from a parts list of regulatory elements to an integrated splicing code. RNA **14:**802–813.
62. **Xie, J., J. A. Lee, T. L. Kress, K. L. Mowry, and D. L. Black.** 2003. Protein kinase A phosphorylation modulates transport of the polypyrimidine tract-binding protein. Proc. Natl. Acad. Sci. U. S. A. **100:**8776–8781.
63. **Xing, Y., and C. Lee.** 2007. Relating alternative splicing to proteome complexity and genome evolution. Adv. Exp. Med. Biol. **623:**36–49.
64. **Xue, Y., et al.** 2009. Genome-wide analysis of PTB-RNA interactions reveals a strategy used by the general splicing repressor to modulate exon inclusion or skipping. Mol. Cell **36:**996–1006.
65. **Yeo, G. W., E. L. Nostrand, and T. Y. Liang.** 2007. Discovery and analysis of evolutionarily conserved intronic splicing regulatory elements. PLoS Genet. **3:**e85.
66. **Yu, Y., et al.** 2008. Dynamic regulation of alternative splicing by silencers that modulate 5′ splice site competition. Cell **135:**1224–1236.
67. **Zhang, D., and M. Rosbash.** 1999. Identification of eight proteins that cross-link to pre-mRNA in the yeast commitment complex. Genes Dev. **13:**581–592.
68. **Zhang, T., N. Delestienne, G. Huez, V. Kruys, and C. Gueydan.** 2005. Identification of the sequence determinants mediating the nucleo-cytoplasmic shuttling of TIAR and TIA-1 RNA-binding proteins. J. Cell Sci. **118:**5453–5463.
69. **Zhang, X. H., C. S. Leslie, and L. A. Chasin.** 2005. Dichotomous splicing signals in exon flanks. Genome Res. **15:**768–779.
70. **Zhang, Z., et al.** 2008. SMN deficiency causes tissue-specific perturbations in the repertoire of snRNAs and widespread defects in splicing. Cell **133:**585–600.
71. **Zuccato, E., E. Buratti, C. Stuani, F. E. Baralle, and F. Pagani.** 2004. An intronic polypyrimidine-rich element downstream of the donor site modulates cystic fibrosis transmembrane conductance regulator exon 9 alternative splicing. J. Biol. Chem. **279:**16980–16988.